

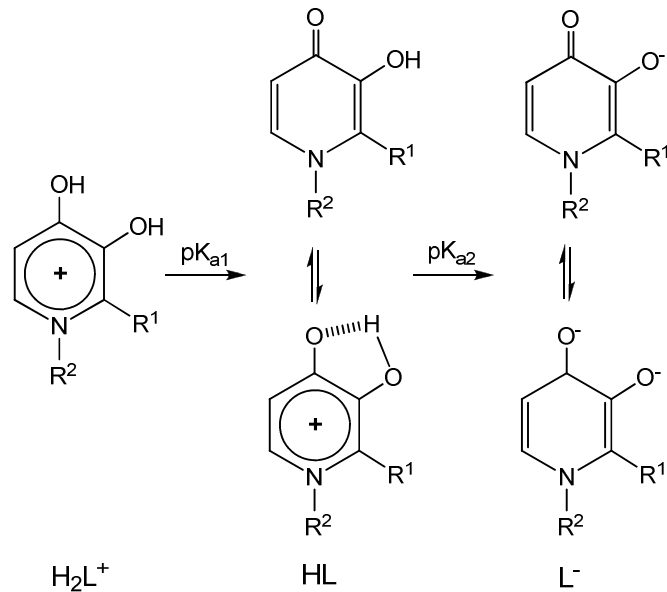
Electronic Supplementary Information

Spectroscopic and Potentiometric Characterization of Vanadium (IV) and (V) complexes of a heterocyclic 5-hydroxy-4-pyrimidinone

Gisela Gonçalves, Isabel Tomaz, Isabel Correia, Luís F. Veiros, M. Margarida C.A. Castro, Fernando Avecilla* Lorena Palacio, Miguel Maestro, Tamás Kiss, Tamás Jakusch, M. Helena V. Garcia, João Costa Pessoa,*

ESI-1 - Protonated/deprotonated forms of mhcpes calculated by DFT

For pyridinones it is normally assumed that the protonation of the HL form takes place mainly on the carbonyl-O atom rather than on the N atom of the ring²⁸ (see scheme SI-1-1), and the deprotonation of the HL form yields L⁻, which is considered to have partial negative charges on both O atoms.



Scheme S-1-1 - Deprotonation steps of pyridinones (from²⁷)

With mhcpes the situation is more complex, as for each stoichiometry H_2L^+ , HL and L^- several tautomers may be postulated for each, and intramolecular H-bond formation involving atoms $\text{O}(2)-\text{H}(3)\cdots\text{O}(3)$ or $\text{O}(1)-\text{H}(25)\cdots\text{O}(2)$ or $\text{O}(2)-\text{H}(3)\cdots\text{O}(1)$ may contribute to stabilize particular forms.

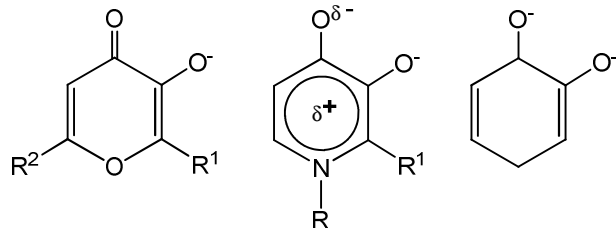
The stability of the several tautomers considered may depend, to some extent, on solvation and ionic interactions occurring in solution. Since the solvent is water, solvation will rely on H-bonds established between solute and solvent, and an accurate model for such a system requires the explicit consideration of, at least, the solvent molecules involved in the first solvation layer. Our computational limitations preclude the use of a model of that size, and, thus, the relative energies calculated should be taken with due caution. However, since the comparison is made between isomers, part of the solvation effects are expected to cancel, and the energy differences calculated with implicit solvent corrections (PCM model, see Computational details) should give important clues to understand the predominant species in aqueous solution, in each case.

The performance of the theoretical method employed may be tested through the comparison between the X-ray structure obtained for mhcpe, and the corresponding optimized structure. Values of 0.02 and 0.04 Å are obtained for the mean and maximum absolute deviations, respectively, for all bonds between non-hydrogen atoms, indicating a very good agreement between the calculated and the experimental structure, and validating the theoretical approach, in what concerns the structural description of the system.

The structures of other tautomeric forms were calculated in a thorough search for each stoichiometry H_2L^+ (a total of 8 tautomers), HL (a total of 10 tautomers) and L^- (a total of 5 tautomers). The structures presented in Scheme 2 and discussed above correspond to the most stable tautomers, with energy differences inferior to 10 kcal mol⁻¹ with respect to the most stable tautomer of each stoichiometry. This 10 kcal mol⁻¹ cutoff was established at the PBE1PBE/6-31G(d,p) level. Single point energy calculations at the PBE1PBE/6-311++G(d,p)//PBE1PBE/6-31G(d,p) level were performed only for the tautomers presented in Scheme 3 (see text for Computational details). From the DFT calculations for the pyrimidinone mhcpe, for the set of most stable tautomers found, as far as H-bond formation is concerned, the H-bond O(2)–H···O(3) is normally the most relevant one, and only in one case (structure **DFT-7**) the H-bond O(1)–H(25)···O(2) is important. For the set of most stable tautomers found, the H-bond O(2)–H(3)···O(1) is never relevant.

A classical way of evaluating the charges of the atoms and the capacity of donor atoms to coordinate to metal ions is to establish schemes such as Scheme S-1-2,²⁸ where the relevant resonance contributors are shown. Similar schemes may be considered for mhcpe, but it is not possible to anticipate their relative importance. DFT calculations may help in this respect supplying the partial charges calculated for the atoms for the most stable tautomers found for each stoichiometry H_2L^+ , HL and L^- . However, the calculated partial charges do not give adequate

information about which may be the relevant resonance contributors, as the charges attributed to each atom depend on the type of atoms to which it is bound.



Scheme S-1-2 - Resonance forms of pyrone, pyridinones and catechol ligands (from ref. ²⁸)

A much better indicator of the relevant resonance contributors is the Wiberg Index, calculated by DFT, which gives a measure of the bond order for each bonds. Wiberg indices are electronic parameters related to the electron density between atoms. They can be obtained from a Natural Population Analysis and also provide an indication of the bond strength. Scheme-S-1-3 to -5 specifies the calculated Wiberg Indexes for the most stable tautomers found for each stoichiometry H_2L^+ , HL and L^- . It is interesting to note that the H-bond $\text{O}(2)-\text{H}(3)\cdots\text{O}(3)$ is relevant in most cases, except for **DFT-7** where the H-bond involving $\text{O}(1)-\text{H}(25)\cdots\text{O}(2)$ is the strongest of all shown, explaining why this tautomer is the most stable one for L^- . This H-bond is not relevant in other structures, *e.g.* **DFT-1, -4 or -5**.

As may be anticipated from the DFT-calculated structures, partial charges and Wiberg indexes, globally mhcep is a compound with a variety of possibilities of forming intramolecular and intermolecular hydrogen bonds, this probably being important for the type of interactions established with hTF and HSA.

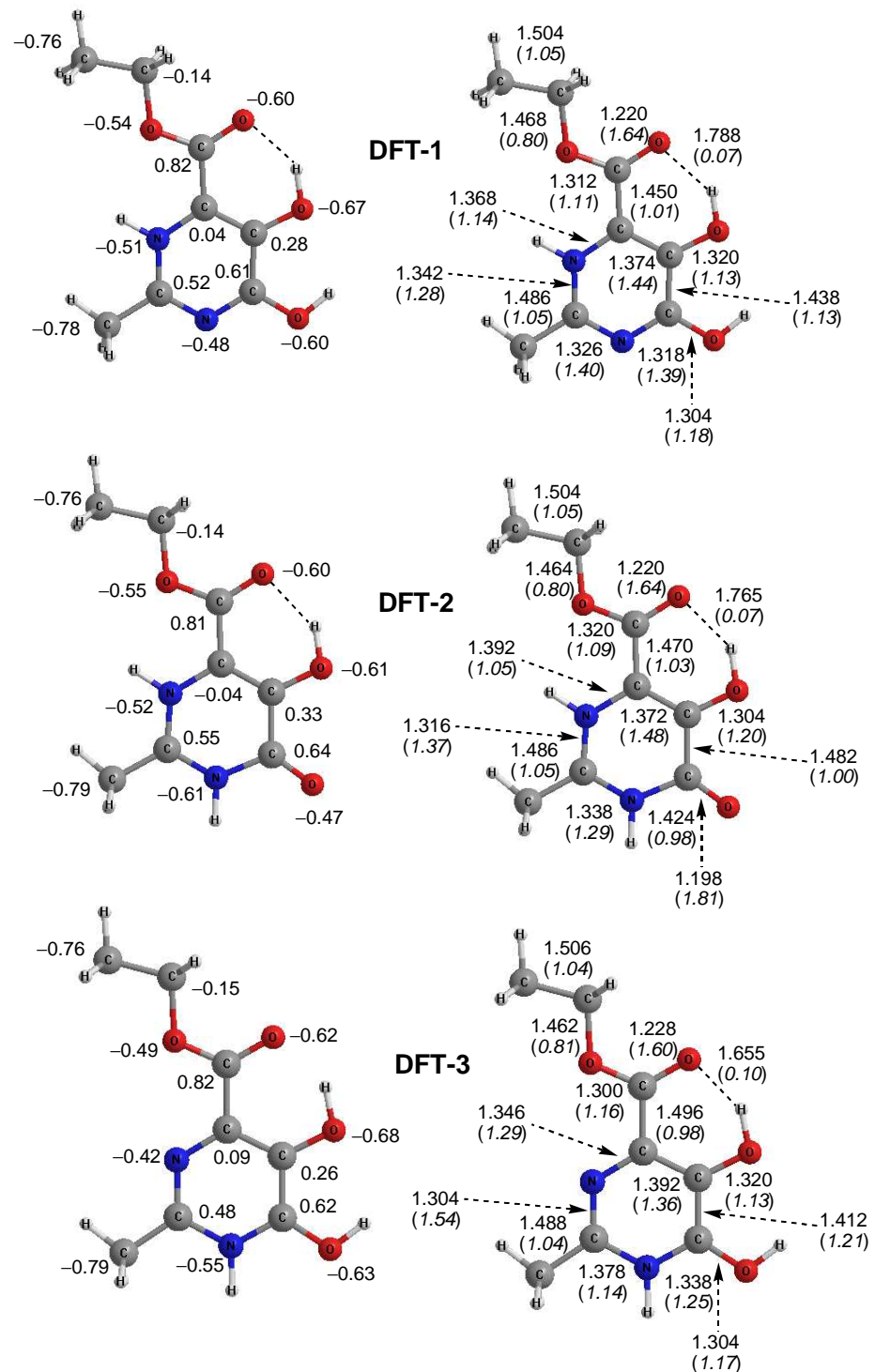


Figure S-1-3. Relevant metric and electronic data for the more stable H_2L^+ species. Left side: NPA atomic charges; Right side: bond distances (\AA) and Wiberg indices (italics).

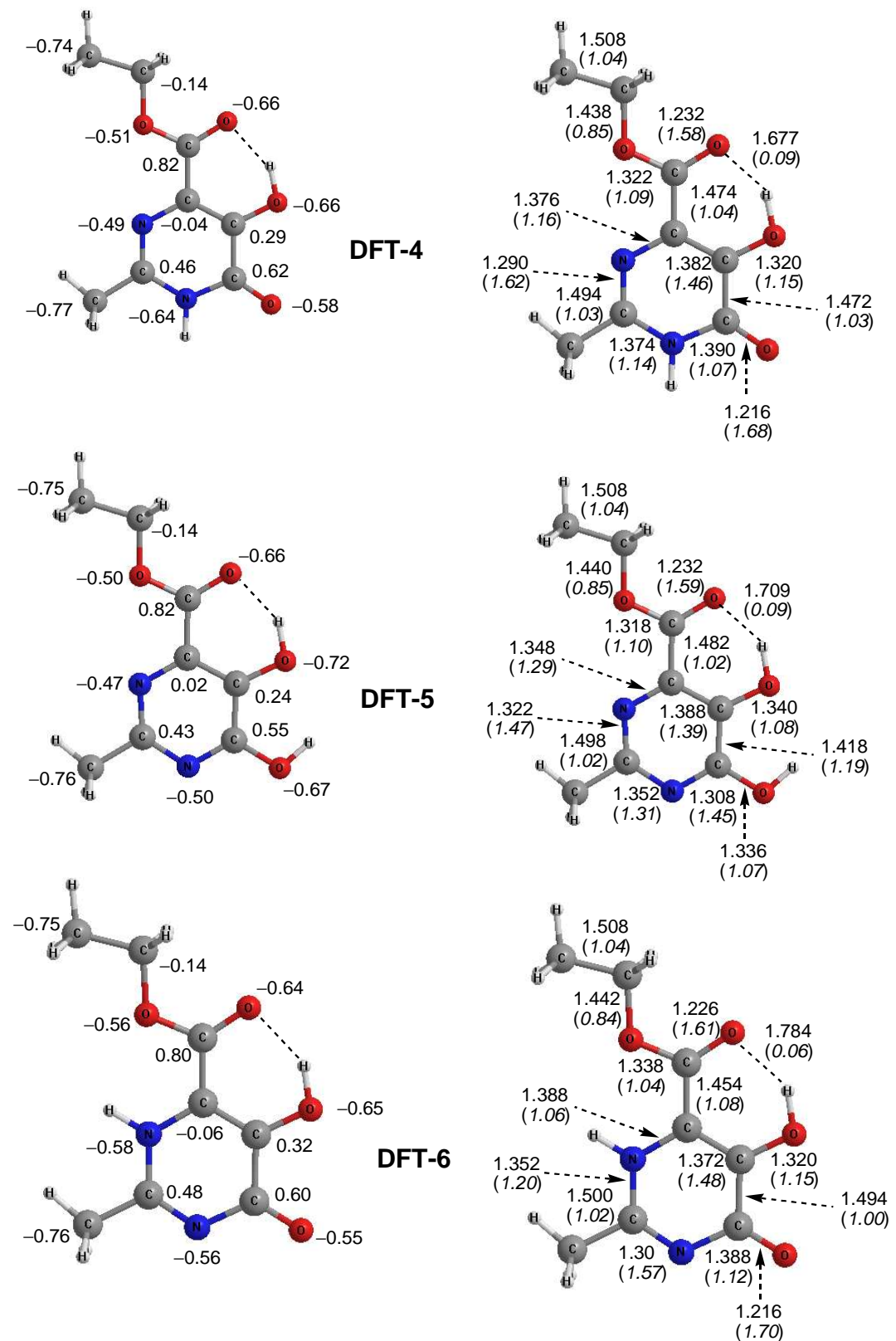


Figure S-1-4. Relevant metric and electronic data for the more stable HL species. Left side: NPA atomic charges; Right side: bond distances (\AA) and Wiberg indices (italics).

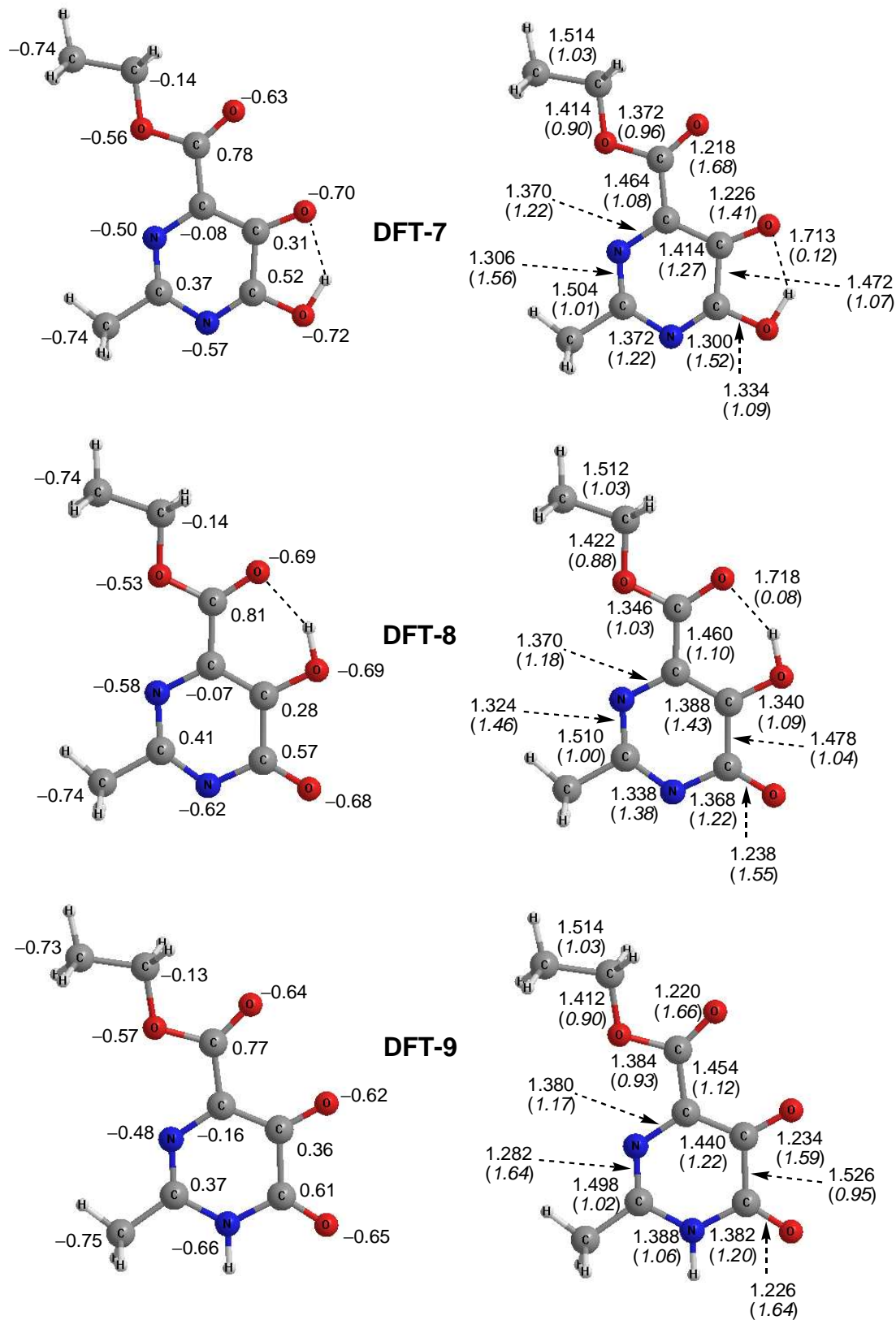


Figure S-1-5. Relevant metric and electronic data for the more stable L^- species. Left side: NPA atomic charges; Right side: bond distances (\AA) and Wiberg indices (italics).

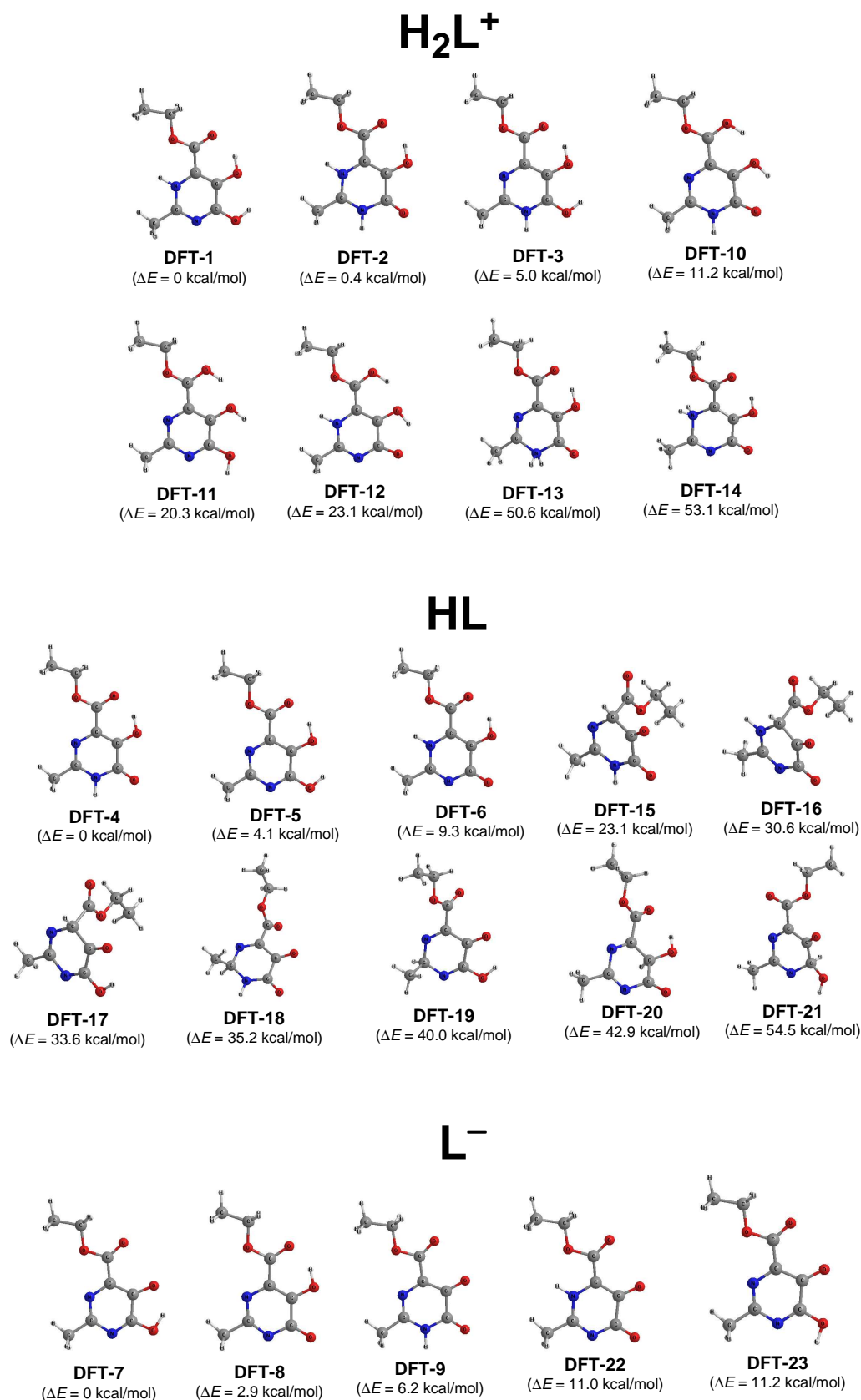


Figure S-1-6. Representation of the optimized geometry of all tautomers considered. Energy differences (PBE1PBE/6-31G**) relative to the most stable tautomer of each stoichiometry are presented.

Atomic coordinates for all the optimized species (PBE1PBE/6-31G**) H₂L⁺ species

DFT-1				DFT-2			
O	-1.862516	2.612602	2.606643	O	-1.895726	2.780800	2.861779
O	0.743720	2.010700	2.302969	O	0.781496	2.168479	2.556844
H	1.646586	1.687070	2.062052	H	1.673162	1.827333	2.292999
O	2.467432	0.603794	0.900340	O	2.485906	0.758243	1.147680
O	1.669357	-0.692910	-0.777127	O	1.642139	-0.524868	-0.517744
N	-2.463166	1.268421	0.907959	N	-2.419785	1.392630	1.124291
H	-0.626448	-0.584727	-1.014570	H	-0.576147	-0.423348	-0.753105
N	-0.867381	0.067680	-0.273778	N	-0.854646	0.224986	-0.022879
C	-1.513349	1.778306	1.666611	C	-1.508763	2.022447	2.019505
C	-0.126350	1.444413	1.488057	C	-0.103720	1.626950	1.769627
C	0.163246	0.560362	0.478260	C	0.173525	0.743411	0.759020
C	-2.144203	0.418097	-0.057014	C	-2.123283	0.532562	0.144163
C	1.561648	0.154999	0.218416	C	1.556810	0.327725	0.484962
C	-3.217025	-0.154674	-0.909979	C	-3.191496	-0.043730	-0.711562
H	-2.832099	-0.832296	-1.673880	H	-2.777199	-0.716252	-1.463775
H	-3.765599	0.659701	-1.391790	H	-3.737143	0.755749	-1.222740
H	-3.930863	-0.690414	-0.277553	H	-3.903913	-0.604380	-0.097962
C	3.022476	-1.153499	-1.108276	C	2.984914	-0.996670	-0.862869
H	3.424107	-1.642520	-0.217296	H	3.393233	-1.491991	0.021557
H	3.624392	-0.266121	-1.318880	H	3.595105	-0.116238	-1.078610
C	2.910446	-2.080851	-2.286876	C	2.852984	-1.920982	-2.042425
H	3.909356	-2.438697	-2.549840	H	3.845277	-2.288359	-2.316829
H	2.496382	-1.569391	-3.159296	H	2.435065	-1.403917	-2.909910
H	2.292646	-2.951467	-2.053221	H	2.229191	-2.786361	-1.804413
H	-1.081192	2.919721	3.096668	H	-3.390085	1.650181	1.278300
DFT-3				DFT-10			
O	-1.829690	2.634167	2.642100	O	-1.776698	2.806832	2.771523
O	0.777996	1.971507	2.265216	O	0.753743	2.148504	2.383687
H	1.659764	1.601866	1.965904	H	2.185646	1.377905	1.688471
O	2.398136	0.594196	0.879930	O	2.463746	0.750248	0.984141
O	1.666243	-0.710692	-0.804008	O	1.669759	-0.506145	-0.645529
N	-2.416735	1.277901	0.927196	N	-2.455567	1.439065	1.027978
H	-3.377986	1.557706	1.109434	H	-3.426847	1.692377	1.177344
N	-0.909878	0.030313	-0.326038	N	-0.902736	0.198316	-0.212413
C	-1.464936	1.802706	1.706047	C	-1.541479	2.021521	1.869239
C	-0.125017	1.427306	1.470165	C	-0.166414	1.607628	1.591535
C	0.087444	0.528089	0.428549	C	0.087083	0.724948	0.575319
C	-2.138823	0.391234	-0.089502	C	-2.125304	0.554581	0.020626
C	1.506616	0.126936	0.175981	C	1.457198	0.312891	0.300313
C	-3.284363	-0.123582	-0.886493	C	-3.251069	0.021909	-0.796380
H	-2.898442	-0.801293	-1.646664	H	-2.852325	-0.653929	-1.551228
H	-3.822811	0.692464	-1.380081	H	-3.791116	0.834613	-1.293435
H	-3.993780	-0.668293	-0.254310	H	-3.964263	-0.523343	-0.169227
C	3.036044	-1.131987	-1.088116	C	3.046857	-0.948850	-0.953999
H	3.430066	-1.602078	-0.182951	H	3.434018	-1.424914	-0.049876
H	3.623114	-0.231981	-1.289991	H	3.628997	-0.048481	-1.164480
C	2.982497	-2.072672	-2.261132	C	2.954003	-1.884225	-2.125248
H	3.996579	-2.406656	-2.495904	H	3.961707	-2.228851	-2.372866
H	2.572513	-1.579049	-3.145284	H	2.539730	-1.382440	-3.002181
H	2.377002	-2.953366	-2.034723	H	2.342975	-2.757806	-1.888689
H	-1.045455	2.939657	3.131875	H	0.277457	2.737247	3.011774
DFT-11				DFT-12			
O	-1.824628	2.652939	2.658619	O	-1.714254	2.779247	2.750276
O	0.772490	1.989608	2.279826	O	0.720418	2.148701	2.373790
H	2.159376	1.230095	1.595455	H	2.214272	1.381653	1.690583
O	2.451474	0.602855	0.892407	O	2.492679	0.753524	0.986120
O	1.663616	-0.653560	-0.737952	O	1.695238	-0.513172	-0.650239
N	-2.499443	1.290125	0.922010	N	-2.532976	1.449264	1.032182
H	-2.780094	2.814437	2.699050	H	-0.729964	-0.422531	-0.927030
N	-0.891611	0.052172	-0.302434	N	-0.919027	0.228516	-0.177921
C	-1.564501	1.796133	1.675826	C	-1.570645	1.987815	1.826286
C	-0.197488	1.469462	1.503062	C	-0.162652	1.593988	1.573630
C	0.069650	0.576101	0.477561	C	0.142192	0.716344	0.571748
C	-2.137161	0.422583	-0.057756	C	-2.196512	0.612904	0.082985
C	1.450754	0.163927	0.206088	C	1.486689	0.314510	0.303694
C	-3.233614	-0.134296	-0.898084	C	-3.266878	0.034077	-0.778349
H	-2.829625	-0.809476	-1.651085	H	-2.883830	-0.647378	-1.540664
H	-3.780953	0.677716	-1.385947	H	-3.811432	0.848532	-1.263198
H	-3.951441	-0.670024	-0.269728	H	-3.983157	-0.497136	-0.146105

C	3.041071	-1.097817	-1.046249	C	3.076146	-0.960284	-0.962563
H	3.427730	-1.571443	-0.140618	H	3.460773	-1.436155	-0.057695
H	3.622461	-0.197400	-1.258733	H	3.656047	-0.059238	-1.174360
C	2.946950	-2.035745	-2.215167	C	2.983169	-1.896097	-2.132731
H	3.954533	-2.380960	-2.462544	H	3.992150	-2.239178	-2.377714
H	2.531915	-1.535895	-3.092798	H	2.574608	-1.396471	-3.013905
H	2.335823	-2.908528	-1.976087	H	2.377501	-2.774017	-1.897148
H	0.401416	2.594189	2.941776	H	0.157045	2.720982	2.970728
DFT-13				DFT-14			
O	-1.797197	2.925034	2.830100	O	-1.883232	2.539922	2.993629
O	0.851154	2.186829	2.448027	O	0.779054	2.326553	2.392013
H	1.714286	1.765827	2.128400	H	1.683086	2.020753	2.126632
O	2.419404	0.759186	1.123148	O	2.527231	0.878770	1.033089
O	1.631685	-0.571518	-0.512196	O	1.662407	-0.589061	-0.469425
N	-2.527341	1.527059	1.104287	N	-2.478403	1.535721	1.028219
H	-3.013736	2.319672	0.663588	H	-0.983356	-0.978026	0.513615
N	-0.911590	0.212547	-0.076102	N	-0.866292	-0.030639	0.125770
C	-1.432097	2.150675	2.011546	C	-1.537913	1.960055	2.007659
C	-0.080275	1.667425	1.700611	C	-0.097537	1.643884	1.719024
C	0.103781	0.743193	0.695191	C	0.210000	0.676666	0.813112
C	-2.125292	0.514511	0.047452	C	-2.229881	0.661996	0.166110
C	1.498897	0.301645	0.445856	C	1.588468	0.331828	0.479703
C	-3.258121	-0.019519	-0.746380	C	-3.158481	0.172429	-0.880341
H	-2.857469	-0.728058	-1.471546	H	-2.788895	0.426791	-1.881217
H	-3.786800	0.774500	-1.287143	H	-4.127478	0.648203	-0.730751
H	-3.987879	-0.539600	-0.114327	H	-3.282939	-0.915671	-0.832371
C	2.988823	-1.031528	-0.788129	C	3.009588	-0.979970	-0.895624
H	3.377609	-1.484688	0.127892	H	3.533855	-1.354562	-0.013184
H	3.597248	-0.152737	-1.018330	H	3.517900	-0.076778	-1.241886
C	2.909806	-2.004483	-1.933469	C	2.862887	-2.019050	-1.973650
H	3.915037	-2.367952	-2.162316	H	3.857905	-2.326566	-2.305738
H	2.507481	-1.527658	-2.830393	H	2.328882	-1.623513	-2.841553
H	2.285943	-2.864865	-1.679929	H	2.343597	-2.907544	-1.605669
H	-3.222157	1.115105	1.741763	H	-0.577554	-0.185892	-0.850266

HL species

DFT-4			
O	-1.803972	2.616696	2.922994
O	0.843750	1.945341	2.537148
H	1.702819	1.565367	2.220633
O	2.476045	0.551816	1.130812
O	1.681187	-0.727907	-0.532079
N	-2.379391	1.246140	1.190493
H	-3.341760	1.511628	1.357525
N	-0.857516	0.002339	-0.060753
C	-1.463855	1.843242	2.049962
C	-0.084317	1.419978	1.760456
C	0.137637	0.529035	0.728369
C	-2.070891	0.365500	0.183102
C	1.530061	0.125118	0.466914
C	-3.211570	-0.159623	-0.626902
H	-2.818133	-0.838832	-1.382181
H	-3.751197	0.653412	-1.124990
H	-3.927488	-0.701071	0.001299
C	3.032785	-1.137752	-0.804201
H	3.444052	-1.610395	0.093421
H	3.635540	-0.247920	-1.011391
C	2.986102	-2.083741	-1.978207
H	3.997245	-2.423800	-2.219085
H	2.568316	-1.590578	-2.859638
H	2.372552	-2.958991	-1.749701
DFT-5			
O	-1.810244	2.632188	2.644883
O	0.767665	1.971392	2.265015
H	1.638006	1.605562	1.969268
O	2.417349	0.571249	0.854305
O	1.660560	-0.719209	-0.818718
N	-2.473555	1.290035	0.932771
N	-0.906567	0.024167	-0.335063
C	-1.505808	1.775400	1.667452
C	-0.148624	1.420198	1.457999
C	0.086509	0.525966	0.424094
C	-2.133257	0.425011	-0.049134
C	1.491148	0.130069	0.174285
C	-3.261503	-0.113573	-0.872268
H	-2.879787	-0.793968	-1.633484
H	-3.805537	0.705818	-1.351810
H	-3.977197	-0.641248	-0.234462
C	3.018879	-1.120377	-1.079344
H	3.423908	-1.588249	-0.176507
H	3.615040	-0.225243	-1.282289
C	2.988548	-2.068068	-2.252027
H	4.004430	-2.400151	-2.483700
H	2.574173	-1.579337	-3.137372
H	2.380112	-2.947627	-2.027051
H	-0.981550	2.883595	3.078356
DFT-6			
O	-1.841937	2.765570	2.861227
O	0.773021	2.150197	2.536492
H	1.650656	1.802475	2.261720
O	2.501537	0.731509	1.116079
O	1.650659	-0.543430	-0.542775
N	-2.493837	1.409064	1.134627
N	-0.859820	0.215184	-0.038567
C	-1.551822	1.987186	1.974539
C	-0.127504	1.605649	1.741589
DFT-15			
O	-1.113122	-0.348144	2.649316
O	0.445750	1.966441	2.288088
O	2.485225	1.836061	-0.910934
O	1.522337	-0.116785	-0.320373
N	-1.723763	-0.136298	0.467816
N	-0.793449	1.397560	-1.079088
C	-0.997303	0.211135	1.584681
C	-0.064885	1.405173	1.352686
C	0.187675	1.805819	-0.096398

C	0.172573	0.724997	0.734892	C	-1.628905	0.484572	-0.778602
C	-2.139287	0.580798	0.198580	C	1.545595	1.209862	-0.501110
C	1.543429	0.320828	0.471434	C	-2.619239	0.000374	-1.790549
C	-3.190760	-0.020041	-0.684391	H	-2.470544	0.547999	-2.719828
H	-2.775947	-0.690824	-1.441341	H	-3.644996	0.153795	-1.438654
H	-3.743818	0.779749	-1.182357	H	-2.486275	-1.070631	-1.979830
H	-3.904413	-0.574498	-0.070367	C	2.736330	-0.814202	-0.658663
C	2.987152	-0.986433	-0.853845	H	3.559934	-0.374444	-0.088129
H	3.404434	-1.474767	0.031814	H	2.945091	-0.652307	-1.720738
H	3.602193	-0.107667	-1.068665	C	2.527174	-2.271703	-0.331585
C	2.892237	-1.922082	-2.032519	H	3.432364	-2.837177	-0.569856
H	3.890475	-2.281673	-2.296528	H	1.699909	-2.688927	-0.912076
H	2.471018	-1.414366	-2.904368	H	2.307980	-2.405765	0.730983
H	2.268728	-2.788993	-1.797743	H	0.317689	2.890871	-0.133454
H	-0.622467	-0.431932	-0.774727	H	-2.378070	-0.897579	0.596198
DFT-16							
O	-1.080990	-0.325790	2.595552	O	-1.777201	-0.049306	2.702472
O	0.523108	1.905267	2.234646	O	0.185627	1.657073	2.270324
H	-0.772407	1.722191	-1.965281	H	-1.087006	0.397250	3.229031
O	2.497622	1.790877	-1.053998	O	2.128736	1.849864	-0.952080
O	1.572673	-0.134774	-0.321228	O	1.256733	-0.142838	-0.354105
N	-1.843751	-0.156100	0.452540	N	-2.336368	-0.032717	0.498873
N	-0.806341	1.389715	-1.013476	N	-1.111409	1.282224	-1.128308
C	-1.032830	0.208227	1.511196	C	-1.585132	0.354369	1.458468
C	-0.041257	1.372890	1.314378	C	-0.440656	1.303540	1.287558
C	0.254081	1.801104	-0.123203	C	-0.162454	1.718546	-0.131437
C	-1.707726	0.429593	-0.699694	C	-2.053569	0.484844	-0.781087
C	1.588941	1.177244	-0.556758	C	1.224243	1.180057	-0.533388
C	-2.619063	0.023322	-1.819330	C	-3.019538	0.012115	-1.818677
H	-3.005762	0.892876	-2.360005	H	-2.772874	0.437634	-2.790810
H	-3.447206	-0.550168	-1.406574	H	-4.038359	0.292397	-1.532837
H	-2.077531	-0.606822	-2.533557	H	-2.997704	-1.081200	-1.870580
C	2.768458	-0.860252	-0.675304	C	2.487087	-0.791716	-0.730940
H	3.620027	-0.380776	-0.183809	H	3.306547	-0.339441	-0.163967
H	2.916933	-0.775115	-1.756594	H	2.669770	-0.596203	-1.791976
C	2.576448	-2.288393	-0.231461	C	2.330247	-2.263113	-0.439467
H	3.466203	-2.873497	-0.480207	H	3.245764	-2.793168	-0.716524
H	1.715282	-2.742196	-0.728714	H	1.500522	-2.688418	-1.009977
H	2.418347	-2.342187	0.848544	H	2.143216	-2.434357	0.623900
H	0.384442	2.885965	-0.148463	H	-0.068221	2.809864	-0.168568
DFT-18							
O	-1.543262	3.514137	2.314339	DFT-19			
O	0.949562	2.341873	1.755330	O	-1.702960	3.163575	2.373553
H	-3.074849	-0.187546	0.913798	O	0.732203	2.227653	1.912044
O	1.749486	-0.664961	1.659802	H	-3.001302	-0.363181	0.531601
O	1.584431	-0.441066	-0.581836	O	1.949460	-0.489627	1.428702
N	-2.487431	1.787851	1.170900	O	1.582648	-0.578680	-0.797273
N	-1.168711	-0.058426	0.263011	N	-2.602888	1.585571	1.004677
C	-1.438095	2.474439	1.699586	N	-1.078422	-0.110577	-0.036818
C	-0.088101	1.809559	1.446803	C	-1.590522	2.108283	1.570159
C	-0.125022	0.483258	0.750244	C	-0.191345	1.620786	1.398966
C	-2.451849	0.557960	0.395487	C	-0.072655	0.411530	0.551555
C	1.181623	-0.269453	0.672956	C	-2.390262	0.464089	0.135407
C	-3.035335	0.774483	-1.001626	C	1.273112	-0.261082	0.456133
H	-3.049318	-0.171063	-1.546968	C	-2.940126	0.795322	-1.258505
H	-2.425738	1.496200	-1.551296	H	-2.885644	-0.084209	-1.902302
H	-4.056825	1.158257	-0.930354	H	-2.351120	1.601015	-1.704955
C	2.817655	-1.171534	-0.733490	H	-3.975024	1.128184	-1.165330
H	2.682857	-2.171905	-0.310377	C	2.830676	-1.278454	-0.959268
H	3.594295	-0.668095	-0.149638	H	2.777776	-2.218282	-0.400567
C	3.141140	-1.212056	-2.205989	H	3.629527	-0.676517	-0.514742
H	4.072171	-1.763557	-2.364210	C	3.034701	-1.502667	-2.436777
H	3.267801	-0.202612	-2.605898	H	3.973708	-2.038091	-2.602913
H	2.346345	-1.709992	-2.767546	H	3.081869	-0.551389	-2.973259
H	-3.389826	2.221348	1.321873	H	2.219622	-2.096945	-2.857786
DFT-20							
O	-0.930928	3.494816	3.015449	DFT-21			
O	1.064238	2.248483	1.668274	O	-1.316771	1.025198	3.255079
H	1.635574	1.688992	1.121314	O	1.018913	0.993284	1.748570
O	1.324344	0.556903	-0.452793	H	-1.430794	-0.664210	2.058236
O	-0.503089	0.655020	-1.761498	O	1.334071	0.556349	-2.056646
N	-2.445055	1.832489	2.591080	O	1.745604	-0.933615	-0.409191
N	-2.022203	0.794625	0.457524	N	-2.488980	0.887035	1.239346
C	-1.167125	2.423520	2.525510	N	-1.296076	0.489551	-0.814683
C	-0.124444	1.559515	1.827920	C	-1.340285	0.446419	1.997927

C	-0.774030	1.048892	0.553528	C	-0.181549	0.356453	-0.201225
C	-2.791643	1.060767	1.625498	C	-2.422643	0.880659	-0.035627
C	0.129930	0.734967	-0.608352	C	1.050321	0.027468	-1.013210
C	-4.119820	0.389689	1.622972	C	-3.589353	1.301185	-0.863951
H	-3.989439	-0.689976	1.492298	H	-3.296759	2.118780	-1.530516
H	-4.702461	0.738131	0.763657	H	-4.415539	1.615965	-0.227202
H	-4.654656	0.597515	2.548801	H	-3.905087	0.471889	-1.505173
C	0.318075	0.333557	-2.903700	C	2.961739	-1.329212	-1.071866
H	0.788975	-0.638544	-2.727715	H	3.597429	-0.445160	-1.180548
H	1.115609	1.079368	-2.977440	H	2.712101	-1.683167	-2.077180
C	-0.579349	0.327399	-4.114996	C	3.608699	-2.399514	-0.229275
H	0.007865	0.085226	-5.005107	H	4.543061	-2.722300	-0.696965
H	-1.042007	1.306337	-4.263316	H	2.954958	-3.270288	-0.131764
H	-1.371517	-0.418163	-4.010500	H	3.835743	-2.022195	0.771042
H	-0.021743	0.662372	2.477591	H	-2.237111	1.223904	3.466279

L⁻ species

DFT-7	DFT-8						
O	-1.820829	2.775809	2.900814	O	-1.804047	2.783912	2.893386
O	0.599466	2.240713	2.650287	O	0.798614	2.112280	2.499266
H	-0.874268	2.910175	3.212209	H	1.644384	1.729642	2.177928
O	2.545113	0.662220	1.090482	O	2.460699	0.698771	1.072551
O	1.630482	-0.578156	-0.547707	O	1.646765	-0.572418	-0.583769
N	-2.506774	1.414629	1.171086	N	-2.487387	1.430625	1.162772
N	-0.825560	0.193756	-0.015453	N	-0.887592	0.162573	-0.105765
C	-1.565659	1.914555	1.916219	C	-1.545320	1.989109	1.981166
C	-0.126023	1.632096	1.809780	C	-0.149184	1.583344	1.714676
C	0.166885	0.719503	0.769607	C	0.100570	0.689861	0.683211
C	-2.062868	0.545991	0.207157	C	-2.103901	0.580405	0.203319
C	1.542938	0.305289	0.497837	C	1.481926	0.295435	0.431028
C	-3.135840	-0.043448	-0.665228	C	-3.224201	0.022956	-0.641745
H	-2.685516	-0.714667	-1.399123	H	-2.826980	-0.656317	-1.399537
H	-3.693437	0.742769	-1.189078	H	-3.773630	0.835480	-1.130248
H	-3.867413	-0.600915	-0.067277	H	-3.945702	-0.511400	-0.013515
C	2.948519	-1.000825	-0.836188	C	2.990120	-0.962912	-0.833108
H	3.389593	-1.491488	0.041286	H	3.411457	-1.434743	0.062727
H	3.585256	-0.133831	-1.054513	H	3.602059	-0.076727	-1.039274
C	2.871085	-1.943931	-2.017354	C	2.967550	-1.914106	-2.008113
H	3.868727	-2.307829	-2.286593	H	3.981975	-2.251290	-2.245133
H	2.438890	-1.438018	-2.885734	H	2.547073	-1.424932	-2.891135
H	2.238232	-2.804799	-1.782214	H	2.352351	-2.789750	-1.783088
DFT-9	DFT-22						
O	-1.994493	2.804254	2.878573	O	-2.035041	2.774217	2.839954
O	0.715781	2.225002	2.619028	O	0.652739	2.275573	2.669069
H	-3.396961	1.650627	1.276787	H	-0.454471	-0.373910	-0.681245
O	2.568320	0.680818	1.073993	O	2.647735	0.688611	1.090208
O	1.616944	-0.546628	-0.555657	O	1.600493	-0.517786	-0.524171
N	-2.421551	1.413940	1.149645	N	-2.512915	1.386873	1.105840
N	-0.799353	0.216933	-0.024293	N	-0.755575	0.265588	0.037942
C	-1.559249	2.036077	2.030110	C	-1.629795	2.003082	1.980938
C	-0.084240	1.687300	1.848808	C	-0.114380	1.720009	1.881872
C	0.181523	0.759204	0.780758	C	0.259956	0.805586	0.845936
C	-2.030264	0.529246	0.153767	C	-2.043601	0.567227	0.197827
C	1.545424	0.343349	0.502089	C	1.593010	0.387563	0.559588
C	-3.119929	-0.040396	-0.699472	C	-3.016235	-0.091790	-0.741655
H	-2.663034	-0.708358	-1.430570	H	-2.525626	-0.754932	-1.461596
H	-3.677377	0.740035	-1.237146	H	-3.574475	0.672223	-1.291000
H	-3.852189	-0.611883	-0.111166	H	-3.745802	-0.672786	-0.169536
C	2.928026	-0.973684	-0.853025	C	2.883760	-0.989764	-0.874981
H	3.377485	-1.468516	0.018461	H	3.342823	-1.504880	-0.021522
H	3.570884	-0.112034	-1.076944	H	3.543026	-0.146310	-1.115232
C	2.838253	-1.916238	-2.034934	C	2.724111	-1.920171	-2.058467
H	3.831823	-2.285283	-2.313264	H	3.695909	-2.317684	-2.370244
H	2.401266	-1.407934	-2.899866	H	2.279478	-1.393302	-2.908704
H	2.203011	-2.774631	-1.795881	H	2.073476	-2.763239	-1.805020
DFT-23							
O	-1.936524	2.660773	2.645989				
O	0.703163	2.090668	2.382359				
H	-2.896694	2.691873	2.529388				
O	2.567067	0.530471	0.826671				
O	1.623637	-0.700368	-0.801609				

N	-2.461097	1.286360	0.921683
N	-0.797955	0.076857	-0.258639
C	-1.538081	1.800591	1.681940
C	-0.087224	1.539494	1.600125
C	0.178945	0.607133	0.530008
C	-2.039158	0.418000	-0.048416
C	1.551052	0.187230	0.249588
C	-3.112945	-0.168928	-0.919215
H	-2.658178	-0.838686	-1.651776
H	-3.672063	0.612887	-1.449666
H	-3.846352	-0.732615	-0.327933
C	2.935666	-1.129305	-1.099047
H	3.383426	-1.621453	-0.225417
H	3.577100	-0.267212	-1.324533
C	2.844442	-2.074249	-2.278373
H	3.837854	-2.444056	-2.555811
H	2.407299	-1.567643	-3.144029
H	2.208917	-2.931522	-2.036786

ESI-2 - Experimental and calculated Visible absorption spectra for the V^{IV}O-mhcpe system and discussion of the plausible binding modes

Fig. S-2-1 includes representative Vis spectra for pH > 6.6. Globally the Vis spectra change significantly as the pH is increased, except in the pH range ca. 4.5-6.5, and particularly for pH > ca. 7, this indicating significant rearrangement of the binding set.

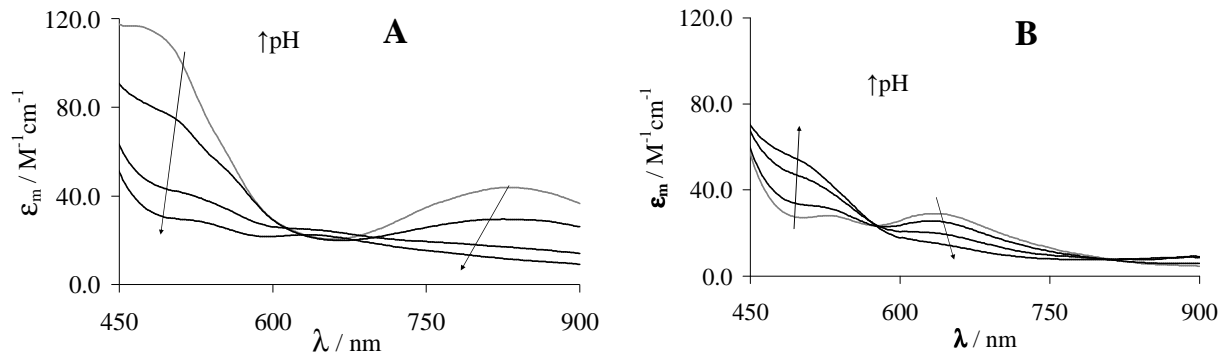


Fig. S-2-1 Visible absorption spectra recorded with aqueous solutions containing V^{IV}O²⁺ and mhcpes: (A) at L:M = 2.76 and $C_{VO} \approx 5 \text{ mM}$ at several pH values (6.68 to 8.22); (B) at L:M = 4.02 at several pH values (9.40 to 11.3) and $C_{VO} \approx 4 \text{ mM}$. Arrows indicate spectral changes upon increasing the pH.

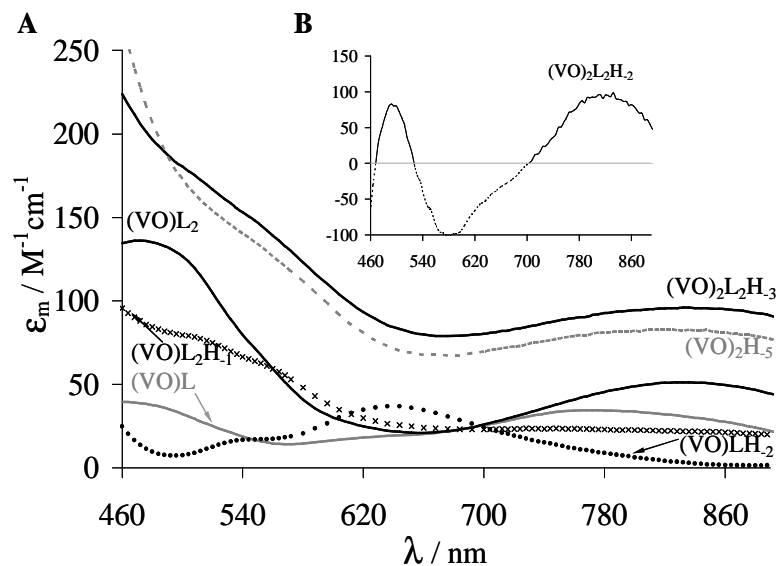


Fig. S-2-2 Calculated visible absorption spectra of each individual species formed in the V^{IV}O-mhcpe system, using the PSEQUAD computer program⁵⁹ with the formation constants listed

in Table 2. The low concentration of species $(VO)_2L_2H_{-2}$ in this system in all experimental conditions limits the accuracy of its calculated spectrum.

For maltol (ma), EPR data is available in several solvents, namely $H_2O/glycerol$ (1:1) and methanol.⁶⁷ In $H_2O/glycerol$ (1:1), for $[V^{IV}O(ma)(H_2O)_2]^+$ the values for g_z , A_z are 1.933, $178 \times 10^{-4} \text{ cm}^{-1}$ and the contribution $(A_z^{O^-})_{\text{maltol}}$ may be back-calculated as $43.3 \times 10^{-4} \text{ cm}^{-1}$. For $[V^{IV}O(ma)_2]$ the g_z , A_z values are 1.938, $171 \times 10^{-4} \text{ cm}^{-1}$,⁶⁷ but as the proportion of *cis* and *trans* isomers is not known, no $A_z^{O^-}$ values can be estimated. In methanol, the coordination geometry is expected to be *cis*- $[V^{IV}O(ma)_2(\text{MeOH})]$, the values for g_z , A_z are 1.939, $169 \times 10^{-4} \text{ cm}^{-1}$, and the average $(A_z^{O^-})_{\text{maltol}}$ is $41.1 \times 10^{-4} \text{ cm}^{-1}$.

For $[V^{IV}O(\text{pyridinones})_2]$ in DMF, where the binding mode is expected to be *trans*, the $g_z = 1.950-1.951$ and $A_z = 158.0 \pm 0.3 \times 10^{-4} \text{ cm}^{-1}$,²⁸ and the $A_z^{O^-}$ may be back-calculated as $39.5 \times 10^{-4} \text{ cm}^{-1}$. For dhp in aqueous solution, the $A_z^{O^-}$ may be back-calculated as (i) $39.3 \times 10^{-4} \text{ cm}^{-1}$ {from $[V^{IV}O(\text{dhp})(H_2O)_2]^+$ }, (ii) as $39.2 \times 10^{-4} \text{ cm}^{-1}$ (from *trans*- $[V^{IV}O(\text{dhp})_2]$), (iii) as $40.1 \times 10^{-4} \text{ cm}^{-1}$ {from *cis*- $[V^{IV}O(\text{dhp})_2]$ } and (iv) as $41.8 \times 10^{-4} \text{ cm}^{-1}$ {from *cis*- $[V^{IV}O(\text{dhp})_2(\text{OH})]^-$ }. This means that the $A_z^{O^-}$ agree well for *trans*- $[V^{IV}O(\text{pyridinones})_2]$, but for dhp complexes the presence of an equatorial H_2O molecule increases the value of $A_z^{O^-}$ by ca. $0.6 \times 10^{-4} \text{ cm}^{-1}$, and the presence of an equatorial HO^- donor increases the value of $A_z^{O^-}$ by ca. $1.5 \times 10^{-4} \text{ cm}^{-1}$.

In the present system, assuming a binding mode ($O^{\delta-}$, $O^{\delta-}$, H_2O , H_2O)_{equat} for $(V^{IV}O)L^+$ the contribution $A_z^{O^-}(\text{mhcpe})$ may be back-calculated as $43.5 \times 10^{-4} \text{ cm}^{-1}$, very close to the corresponding one for maltol ($43.3 \times 10^{-4} \text{ cm}^{-1}$) for the same binding mode (see above). Scheme 3 shows schematic representation of the expected binding set.

For $(V^{IV}O)L_2$ (or ML_2 in Scheme 4), where the A_z is close to the corresponding value for maltol, assuming a *cis* binding mode, *i.e.* a binding set ($3 \times O^{\delta-}$, H_2O)_{equat}($O^{\delta-}$)_{axial}, the $A_z^{O^-}(\text{mhcpe})$ may be back-calculated as $41.9 \times 10^{-4} \text{ cm}^{-1}$, in agreement with the value obtained for *cis*- $[V^{IV}O(\text{ma})_2(\text{MeOH})]$ ($41.1 \times 10^{-4} \text{ cm}^{-1}$).

For $(V^{IV}O)L_2H_{-1}$ (or ML_2H_{-1}) assuming a binding set ($3 \times O^{\delta-}$, HO^-)_{equat}($O^{\delta-}$)_{axial} the contribution $A_z^{O^-}(\text{mhcpe})$ may be back-calculated as $43.4 \times 10^{-4} \text{ cm}^{-1}$. If we assume a decrease of ca. $1.5 \times 10^{-4} \text{ cm}^{-1}$ in the $A_z^{O^-}(\text{mhcpe})$ from $(VO)L_2$ to $(VO)L_2H_{-1}$, as found for dhp,³⁵ a close agreement is also found here for the back-calculated $A_z^{O^-}(\text{mhcpe})$ values.

For $(V^{IV}O)LH_2$ (or MLH_2) two plausible binding sets may be envisaged: $(2\times HO^-$, $2\times O^{\delta-})_{equat}$ and $(2\times HO^-$, $O^{\delta-}$, $H_2O_{equat}(O^{\delta-})_{axial}$. The back-calculated A_z^{O-} (mhcpe) assuming the first possibility corresponds to 44.9×10^{-4} cm $^{-1}$, which agrees well with the increase in A_z^{O-} contribution expected from the insertion of an OH $^-$ donor in the coordination sphere (see above), and we propose it as the most likely coordination mode for this stoichiometry (see Scheme 3).

ESI-3 - Ternary systems V^{IV}O-amino acid-mhcpe

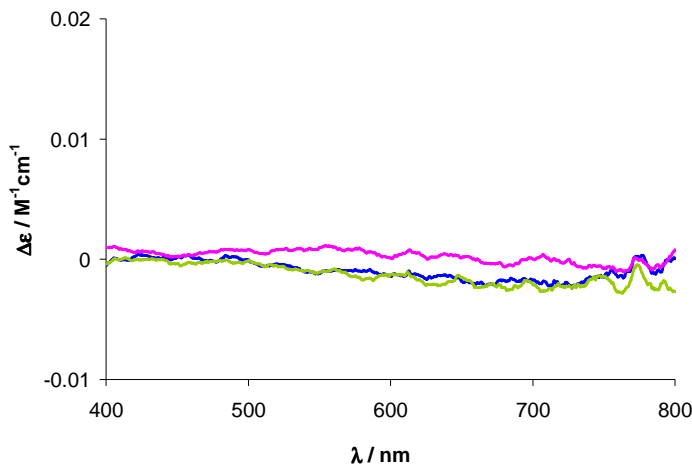


Fig. S-3-1 CD spectra in the 400-800 nm range of solutions containing. (—) L-Tyr ($C_{\text{Tyr}} = 6$ mM), (—) V^{IV}O:mhcpe:L-Tyr = 1:1:3 at pH = 3.0 and (—) V^{IV}O:mhcpe:L-Tyr = 1:1:3 at pH = 7.2. The concentration of L-Tyr is 6 mM (when present, $C_{\text{VO}} = C_{\text{mhcpe}} = 2$ mM). The solvent is water, no buffer was used, optical path = 10 mm.

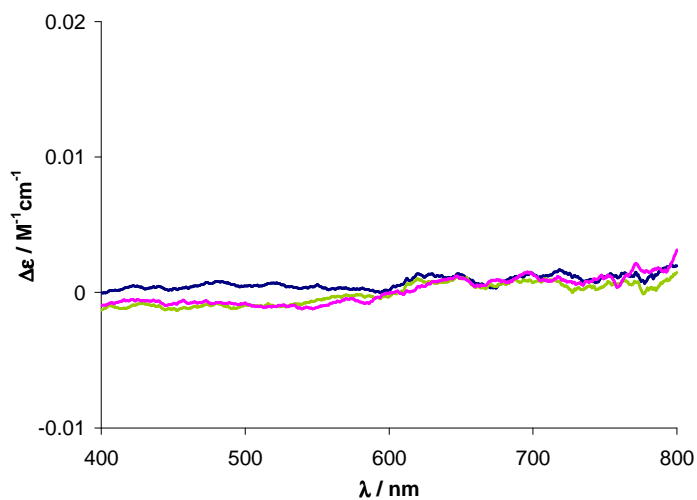


Fig. S-3-2 CD spectra in the 400-800 nm range of solutions containing (—) Gly-L-Asp ($C_{\text{GlyAsp}} = 6$ mM), (—) V^{IV}O:mhcpe:Gly-L-Asp = 1:1:3 at pH = 3.0 and (—) V^{IV}O:mhcpe:Gly-L-Asp = 1:1:3 at pH = 7.2. The concentration of Gly-L-Asp is 6 mM (when present, $C_{\text{VO}} = C_{\text{mhcpe}} = 2$ mM). The solvent is water, no buffer was used, optical path = 10 mm.

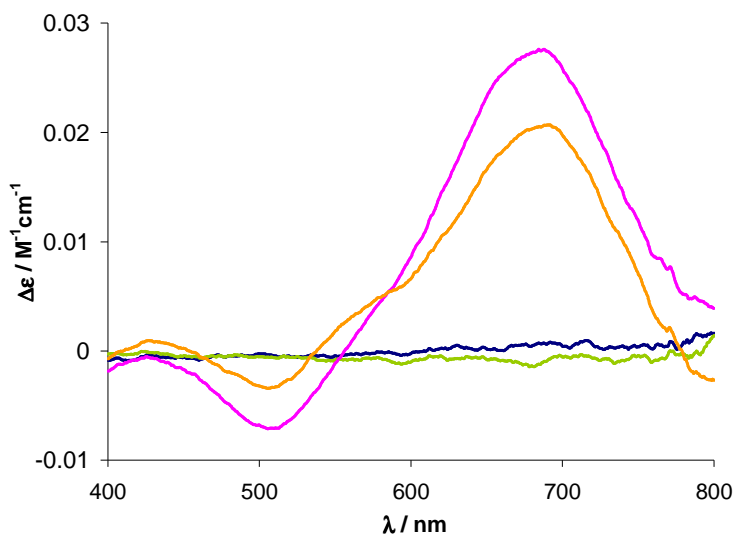


Fig. S-3-3 CD spectra in the 400-800 nm range of solutions containing. (—) L-His ($C_{\text{Tyr}} = 6 \text{ mM}$), (—) $\text{V}^{\text{IV}}\text{O}:\text{mhcpe}:\text{L-His} = 1:1:3$ at pH = 3.0, (—) $\text{V}^{\text{IV}}\text{O}:\text{mhcpe}:\text{L-His} = 1:1:3$ at pH = 7.2 and (—) $\text{V}^{\text{IV}}\text{O}:\text{mhcpe}:\text{L-His}:\text{L-Asp} = 1:1:3:3$ at pH = 7.2. The concentration of L-His or L-Asp is 6 mM (when present, $C_{\text{VO}} = C_{\text{mhcpe}} = 2 \text{ mM}$). The solvent is water, no buffer was used, optical path = 10 mm.

ESI-4 - A 50 mm quartz cell for circular dichroism spectra measurements

For the circular dichroism measurements in the visible range, where for most of the V^{IV}O₄ solutions measured for $\lambda > 500$ nm only bands due to d-d transitions appear, the global absorption is low and the ICD d-d bands are weak. Therefore, because it is not feasible to use high enough concentrations of transferrin or albumin for the measurements, it is important to use quartz cells of high optical path. We used mainly a 50 mm cylindrical quartz cell with a convenient internal diameter of *ca.* 3 mm to keep the sample volume relatively low. A special cell support and modifications in the path of the polarized light had to be done accordingly.

Figure S-4-1 gives a schematic representation of the apparatus.

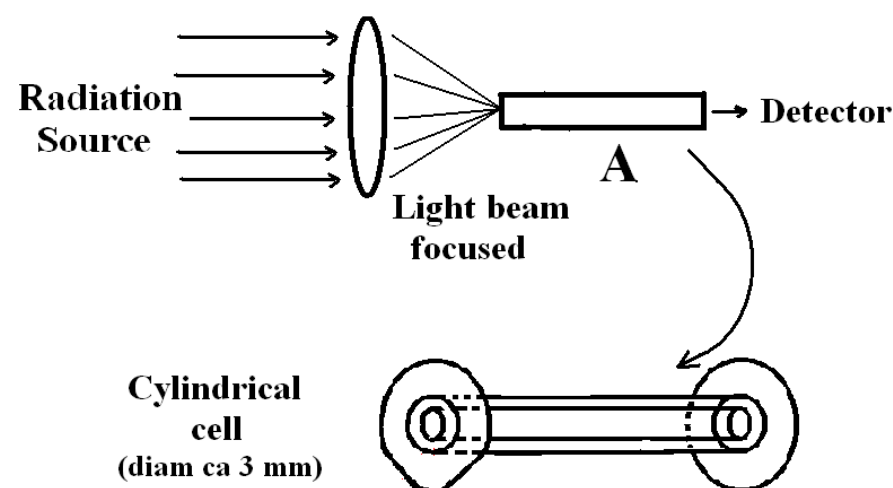


Fig. S-4-1 Schematic representation of the apparatus for measuring CD spectra with the 50 mm quartz cell. Before the entrance of the radiation into the cell, an adequate lens is mounted and the light converges to the middle of the *ca.* 3 mm diameter cell wall. The cell support A and position of the apparatus had to be adequately placed/calibrated to keep the loss of radiation as low as possible. With this apparatus volumes of sample could be reduced to *ca.* 400 μL .

ESI-5 Circular dichroism spectra for the hTF-mhcpe system (UV range)

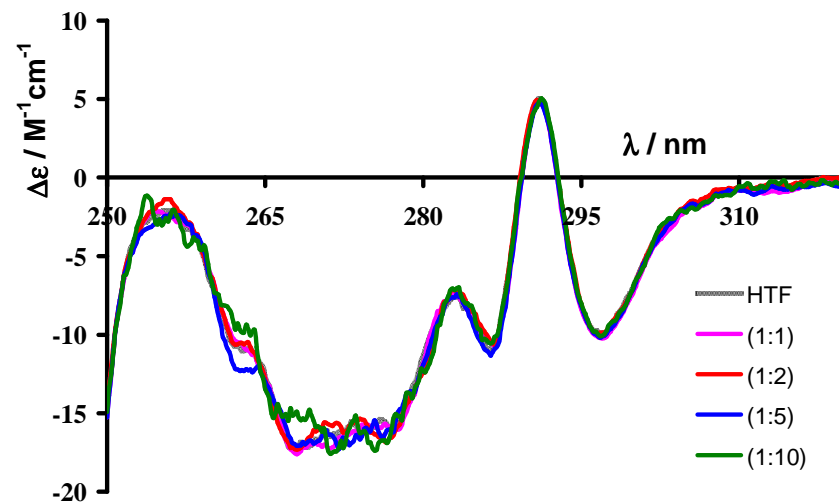


Fig. S-5-1 CD spectra of apo-hTF (100 μ M) solution in Hepes-S buffer at pH 7.4 (●●●●), and after stepwise additions of a mhcppe solution. The molar ratios hTF:mhcpe are indicated. The spectra were recorded with a 2 mm optical path quartz cell. The CD spectra in the range 250-330 nm practically do not change.

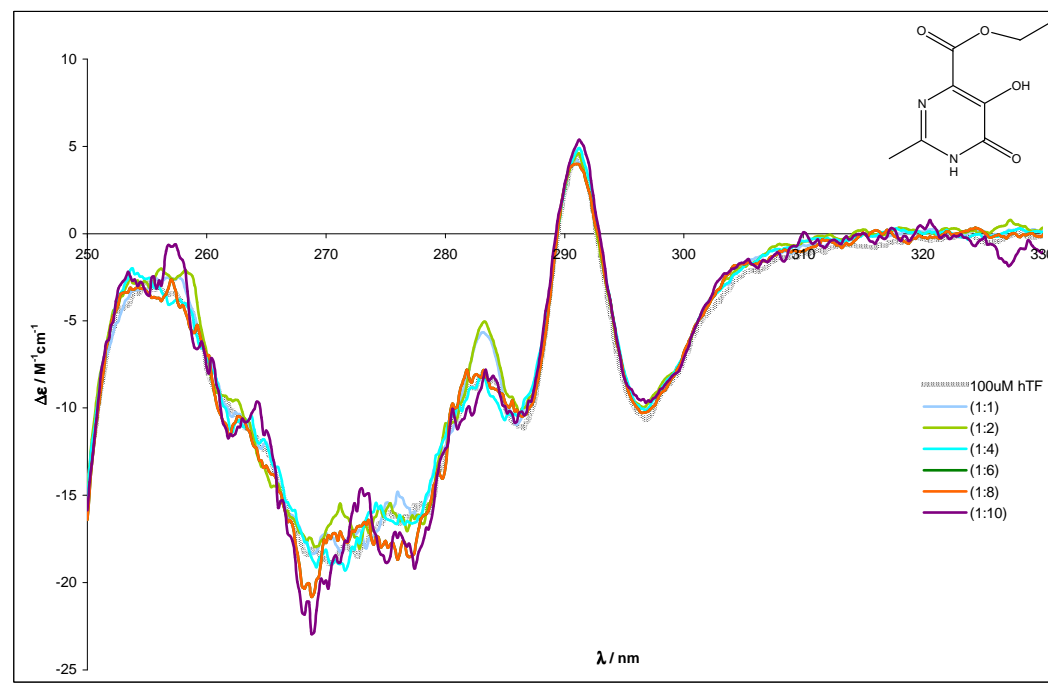


Fig. S-5-2 CD spectra of apo-hTF (100 μ M) solution in Hepes-CL buffer at pH 7.4 (●●●●), and after stepwise additions of a mhcppe solution (color lines). The molar ratios hTF:mhcpe are indicated. The spectra were recorded with a 2 mm optical path quartz cell. The CD spectra in the range 250-330 nm practically do not change and are not significantly different from those recorded in hepes-S buffer as expected (Figure S-5-1).

ESI-6

CD spectra for the apo-hTF (and/or HSA)-V^{IV}OSO₄ – mhcpe (or –maltol, or –dhp systems) in the UV range

Upon the stepwise addition of solutions containing V^{IV}O²⁺ and mhcpe to solutions containing apo-hTF either in HEPES-S or HEPES-CL buffers, significant changes are seen in the CD spectra in the 250-370 nm range, but particularly in the wavelength range 310-370 nm where the protein alone shows no CD signal (see Fig. 7 and Fig. S-6-1). The measurements made in Hepes-CL (Fig. 7) or Hepes-S buffers show similar CD spectra, but the $\Delta\epsilon$ values in the 320-360 nm range are *ca.* 25% higher in the case of Hepes-S buffer, possibly because the citrate and lactate present in the Hepes-CL buffer partly sequester the V^{IV}O²⁺ in the bulk solution, decreasing the amount of metal ion bound to hTF.

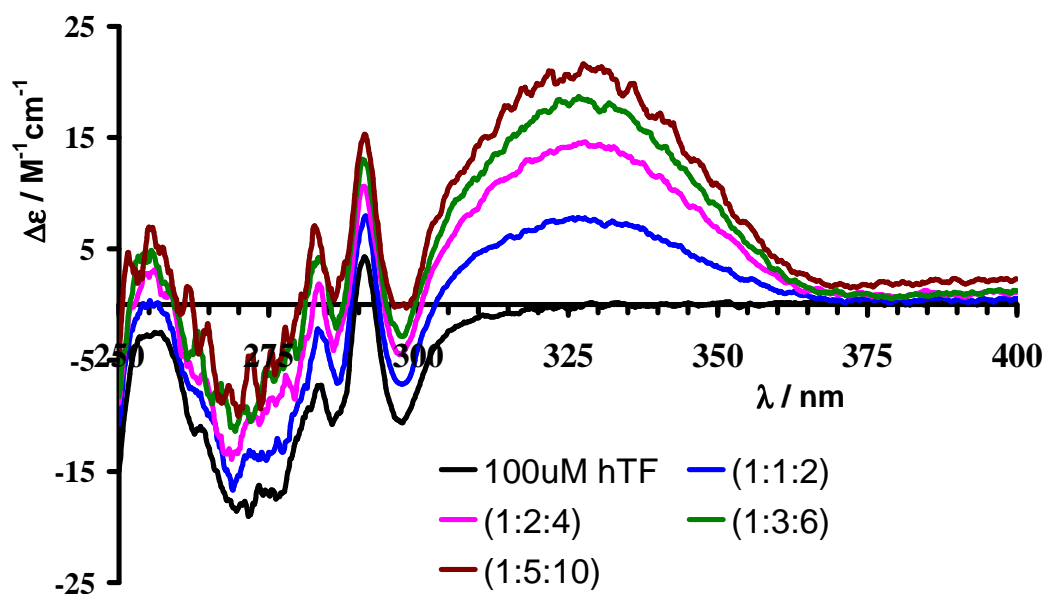


Fig. S-6-1 CD spectra in the 250-400 nm range of solutions containing apo-hTF ($C_{\text{hTF}} = 100 \mu\text{M}$) in Hepes-S buffer at pH 7.4 (black line), and after stepwise additions of a solution containing V^{IV}OSO₄ and mhcpe in 1:2 molar ratio: (a) apo-hTF; (b) apo-hTF:V^{IV}O:mhcpe = 1:1:2 (electric blue); (c) apo-hTF:V^{IV}O:mhcpe = 1:2:4 (magenta); (d) apo-hTF:VO:mhcpe = 1:3:6 (dark green); (e) apo-hTF:VO:mhcpe = 1:6:12. The spectra were recorded with a 2 mm optical path quartz cell. The signal to noise ratio is poorer for $\lambda < 275$ nm due to a substantial increase in the optical density of the sample. For $\lambda < 275$ nm the optical density is too high, consequently the noise of the CD signal increases.

Figures S-6-2 and S-6-3 depict CD spectra for apo-hTF in the range 250-400 nm and after additions of $\text{V}^{\text{IV}}\text{OSO}_4$ and/or Hdhp. Up to *ca.* 300 nm apo-hTF has an intrinsic CD signal, but not for $\lambda > 320$ nm. Any CD signal detected for $\lambda > \text{ca. } 320$ nm is thus an ICD signal due to $\text{V}^{\text{IV}}\text{O}$ -Hdhp complexes in close interaction with the protein.

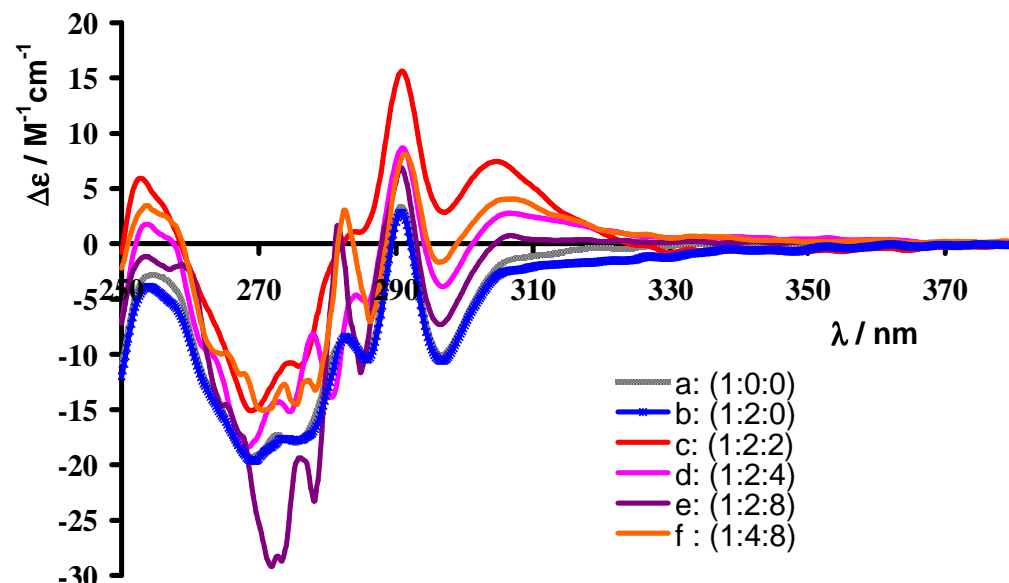
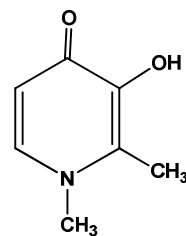


Figure S-6-2 CD spectra in the 250-400 nm range of solutions in Hepes-CL buffer at pH 7.4 containing (a) apo-hTF (grey spectrum, $C_{\text{HTF}} = 100 \mu\text{M}$); (b) apo-hTF and $\text{V}^{\text{IV}}\text{OSO}_4$ (black spectrum, $C_{\text{HTF}} = 100 \mu\text{M}$, $C_{\text{VO}} = 200 \mu\text{M}$); (c)-(e) after stepwise additions of a solution of Hdhp ($C_{\text{HTF}} = 100 \mu\text{M}$ and relative apo-hTF: $\text{V}^{\text{IV}}\text{O}$:dhp concentrations indicated); (f) after addition of both $\text{V}^{\text{IV}}\text{OSO}_4$ and Hdhp ($C_{\text{HTF}} = 100 \mu\text{M}$ and relative apo-hTF: $\text{V}^{\text{IV}}\text{O}$:dhp concentrations of 1:4:8). The spectra were recorded with a 2 mm optical path. For $\lambda < 275$ nm the optical density is too high, consequently the noise in the CD signal increases significantly.



Hdhp

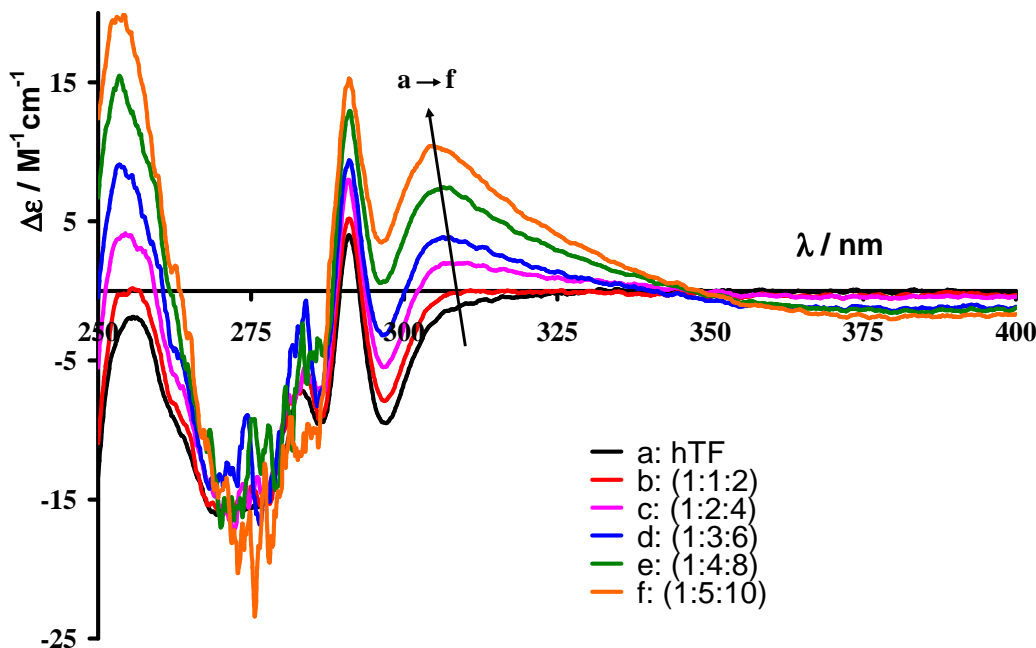
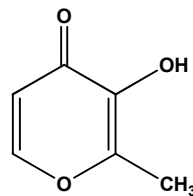


Fig. S-6-3 CD spectra in the 250-400 nm range of solutions in Hepes-CL buffer at pH 7.4 containing (a) apo-hTF alone (grey spectrum, $C_{HTF} = 100 \mu M$); (b-f) the same solution after stepwise additions of a $V^{IV}OSO_4$ -Hdhp solution. The relative apo-hTF: $V^{IV}O$:dhp concentrations (in molar equivalents) are: (b): 1:1:2, (c): 1:2:4, (d) 1:3:6, (e) 1:4:8, (f) 1:5:10. The spectra were recorded with a 2 mm optical path. Depending on the Hdhp concentration, for $\lambda < 270$ -290 nm the optical density is too high, consequently the noise in the CD signal increases significantly.

Figures S-6-4 and S-6-5 depict CD spectra in the range 250-400 nm of solutions containing apo-hTF and after additions of solutions containing $V^{IV}OSO_4$ and/or maltol. Up to *ca.* 300 nm hTF has an intrinsic CD signal, but not for $\lambda > 320$ nm. Any CD signal detected for $\lambda > ca.$ 320 nm is due to $V^{IV}O$ -maltol complexes in close interaction with chiral groups of hTF.



Maltol

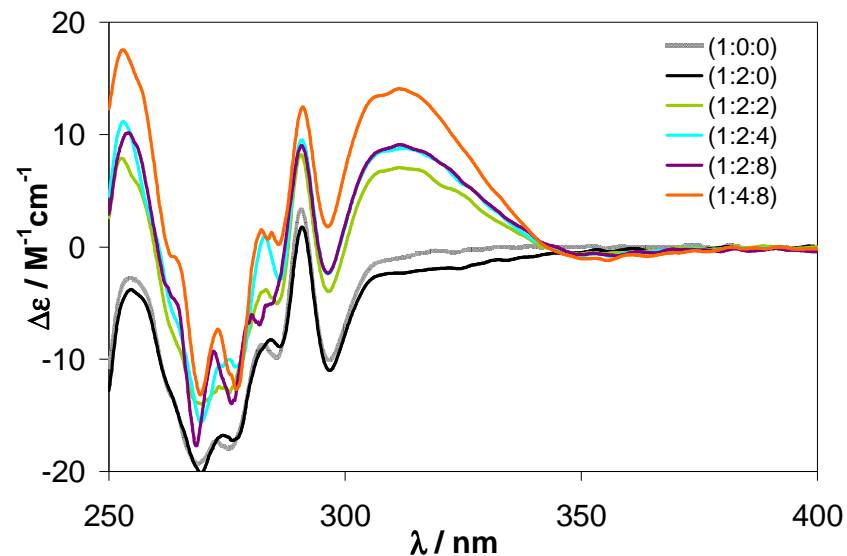


Fig. S-6-4 CD spectra in the 250-330 nm range of solutions in Hepes-CL buffer at pH 7.4 containing (a) apo-hTF (grey spectrum, $C_{HTF} = 100 \mu M$); (b) apo-hTF and $V^{IV}OSO_4$ (black spectrum, $C_{HTF} = 100 \mu M$, $C_{VO} = 200 \mu M$); (c)-(e) after successive additions of a solution of maltol ($C_{HTF} = 100 \mu M$ and relative apo-hTF: $V^{IV}O$:maltol molar ratios indicated); (f) after addition of both $V^{IV}OSO_4$ and maltol ($C_{HTF} = 100 \mu M$ and relative apo-hTF: $V^{IV}O$:maltol concentrations of 1:4:8). For $\lambda < 275$ nm the optical density is too high, consequently the noise of the CD signal increases significantly.

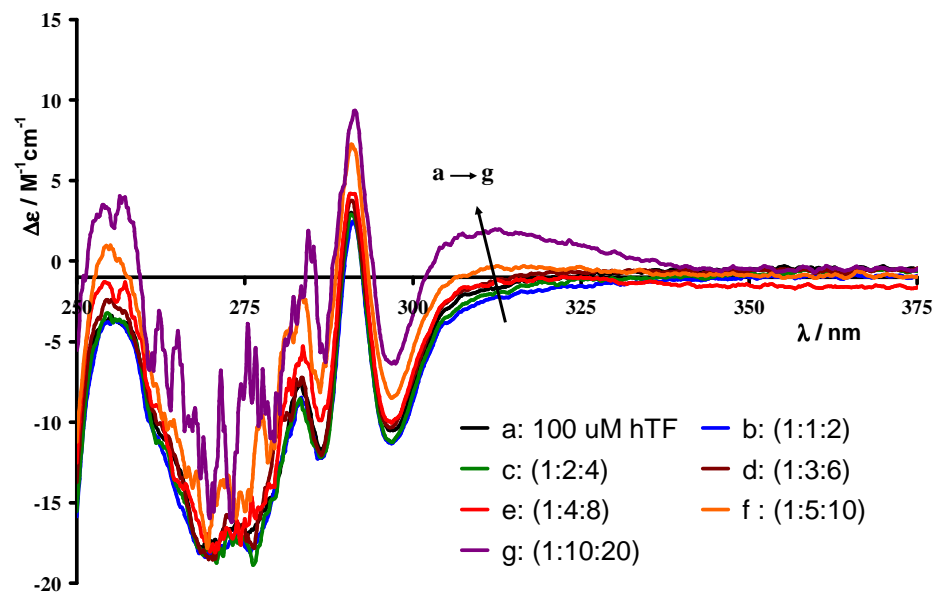


Fig. S-6-5 CD spectra in the 250-400 nm range of solutions in Hepes-CL buffer at pH 7.4 containing (a) apo-hTF (grey spectrum, $C_{HTF} = 100 \mu M$); (b-g) the same solution after stepwise additions of a solution containing $V^{IV}OSO_4$ and maltol. The relative apo-hTF: $V^{IV}O$:maltol concentrations are: (b): 1:1:2, (c): 1:2:4, (d) 1:3:6, (e) 1:4:8, (f) 1:5:10, (g) 1:10:20. The spectra were recorded with a 2 mm optical path. Depending on the maltol concentration, for $\lambda < 270$ -290 nm the optical density is too high, consequently the noise in the CD signal increases significantly.

The changes observed in CD spectra in the UV range clearly show that in all these systems ternary hTF-V^{IV}O-mhcpe, maltol or dhp species are formed, this leading to induced CD signals in ligand-centered electronic transitions in the range 300-370 nm. The changes observed depend on the relative hTF-V^{IV}O-ligand ratios, on the λ_{\max} of the ligand-centered bands and in some cases on the order of addition of reagents. Increasing the ligand:(hTF-V^{IV}O) ratio, particularly for dhp which binds V^{IV}O very strongly,⁴³ there is a trend for an increase in the formation of binary V^{IV}O-ligand species, thereby lower proportions of V^{IV}O are bound to the protein.

Figure S-6-6A depicts the CD spectrum in the range 290-390 nm of a solution containing HSA, and the spectrum of the same sample after additions of a solution containing V^{IV}OSO₄ and dhp in a 1:2 molar ratio. Changes are observed, namely more negative Φ values for $\lambda < 310$ nm, and an increase of Φ values for $\lambda > 310$ nm. Figure S-6-6B depicts CD spectra of solutions containing HSA and apo-hTF in concentrations approximately corresponding to those found in blood serum ($C_{\text{HSA}} = 630 \mu\text{M}$, $C_{\text{hTF}} = 40 \mu\text{M}$).

The changes of the CD signals seen in Fig. S-6-6B upon the stepwise addition of V^{IV}O-dhp complexes (1:2) up to a V^{IV}O-hTF ratio of 1:2 are consistent with the binding of V^{IV}O-dhp complexes mainly to hTF. Upon further additions of V^{IV}O-dhp complexes the CD spectra do not change much. These results therefore indicate that V^{IV}O, in the presence of the dhp ligand, is more strongly bound to hTF than to HSA, but this conclusion is not so straightforward as in the case of mhcppe (Fig. 15 of main text).

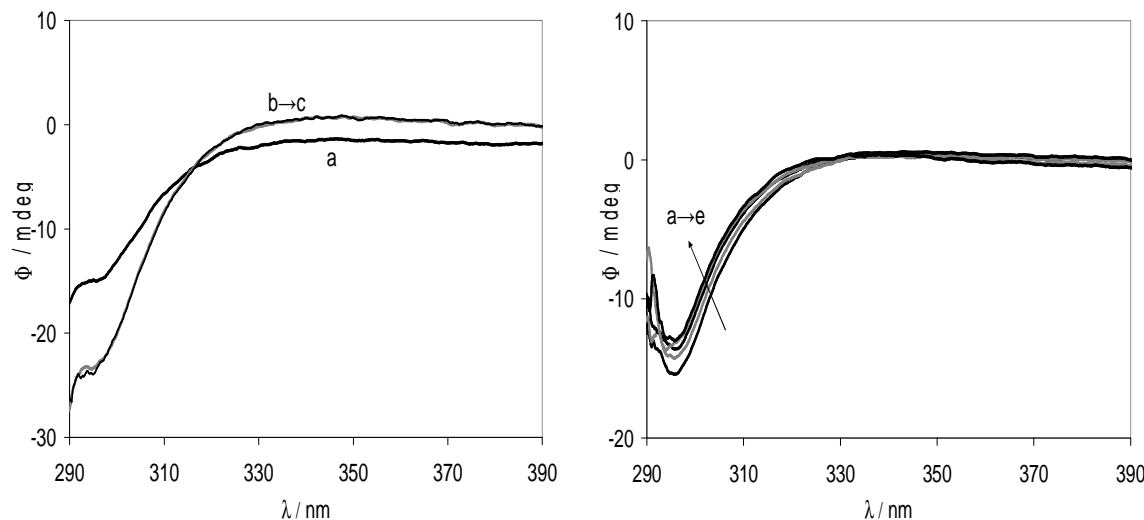


Fig. S-6-6. – (A) CD spectra of HSA solution (a, —, $C_{\text{HSA}} = 0.630 \text{ mM}$), and after additions of a solution containing V^{IV}OSO₄ and dhp (b, —, $C_{\text{HSA}} = 0.630 \text{ mM}$, $C_V = 80 \mu\text{M}$, $C_{\text{dhp}} = 2 \times C_V$), (c, —, $C_{\text{HSA}} = 0.630 \text{ mM}$, $C_V = 160 \mu\text{M}$, $C_{\text{dhp}} = 2 \times C_V$). (B) CD spectra of a solution

containing HSA and apo-hTF (a: $C_{\text{HSA}} = 630 \mu\text{M}$, $C_{\text{hTF}} = 40 \mu\text{M}$), and after stepwise additions of a solution containing $\text{V}^{\text{IV}}\text{OSO}_4$ and dhp: (b: $C_{\text{HSA}} = 0.63 \text{ mM}$, $C_{\text{hTF}} = 40 \mu\text{M}$, $C_{\text{V}} = 40 \mu\text{M}$, $C_{\text{dhp}} = 2 \times C_{\text{V}}$); (c: $C_{\text{HSA}} = 0.63 \text{ mM}$, $C_{\text{hTF}} = 40 \mu\text{M}$, $C_{\text{V}} = 80 \mu\text{M}$, $C_{\text{dhp}} = 2 \times C_{\text{V}}$); (d: $C_{\text{HSA}} = 0.63 \text{ mM}$, $C_{\text{hTF}} = 40 \mu\text{M}$, $C_{\text{V}} = 0.16 \text{ mM}$, $C_{\text{dhp}} = 2 \times C_{\text{V}}$); (e: $C_{\text{HSA}} = 0.63 \text{ mM}$, $C_{\text{hTF}} = 40 \mu\text{M}$, $C_{\text{V}} = 0.32 \text{ mM}$, $C_{\text{dhp}} = 2 \times C_{\text{V}}$). All spectra were recorded with a 2 mm optical path quartz cell in HEPES-S buffer at pH 7.4. The CD signals were corrected for the dilution caused by the addition of the solution containing $\text{V}^{\text{IV}}\text{OSO}_4$ and dhp.

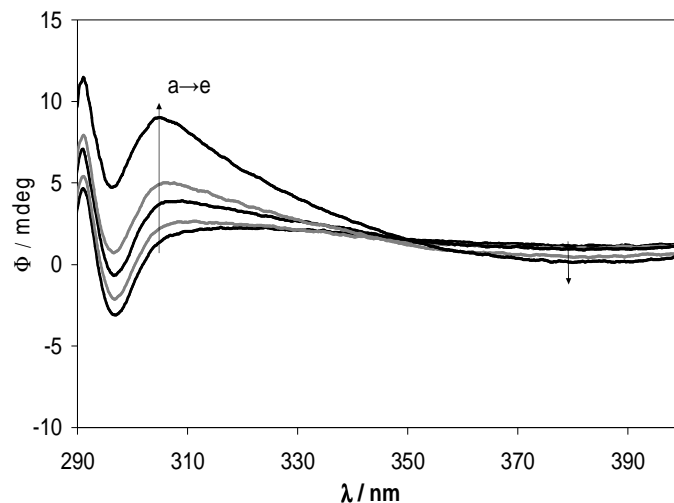


Fig. S-6-7 CD spectra in the 290–400 nm range of solutions containing apo-hTF ($C_{\text{HTF}} = 100 \mu\text{M}$) and after stepwise additions of a solution containing $\text{V}^{\text{IV}}\text{OSO}_4$ and dhp in 1:2 molar ratio in HEPES-CL buffer. (a) apo-hTF; (b) apo-hTF: $\text{V}^{\text{IV}}\text{O}$:dhp = 1:1:2; (c) apo-hTF: $\text{V}^{\text{IV}}\text{O}$:mhcpe = 1:2:4; (d) apo-hTF:VO:dhp = 1:3:6; (e) apo-hTF:VO:dhp = 1:6:12. The spectra were recorded with a 2 mm optical path quartz cell.

Figure S-6-8A depicts the CD spectrum of a solution containing HSA in the range 290–390 nm, and the spectrum of the same sample after additions of a solution containing $\text{V}^{\text{IV}}\text{OSO}_4$ and maltol in a 1:2 molar ratio. Some changes are observed, consistent with interactions with HSA. Figure S-6-8B depicts CD spectra of solutions containing HSA and apo-hTF in concentrations approximately corresponding to those found in blood serum ($C_{\text{HSA}} = 630 \mu\text{M}$, $C_{\text{hTF}} = 40 \mu\text{M}$).

The changes of the CD signals upon the stepwise addition of $\text{V}^{\text{IV}}\text{O}$ -maltol complexes (1:2) up to a $\text{V}^{\text{IV}}\text{O}$ -hTF ratio of 1:2 are consistent with the binding of $\text{V}^{\text{IV}}\text{O}$ -dhp complexes mainly to hTF. Upon further additions of $\text{V}^{\text{IV}}\text{O}$ -maltol complexes, there are no more available hTF binding sites, and the CD spectra then change with a pattern similar to that of Figure S-6-8A, *i.e.* consistent with the binding to HSA. These results therefore demonstrate that $\text{V}^{\text{IV}}\text{O}$, in the presence of the maltol ligand, is more strongly bound to hTF than to HSA.

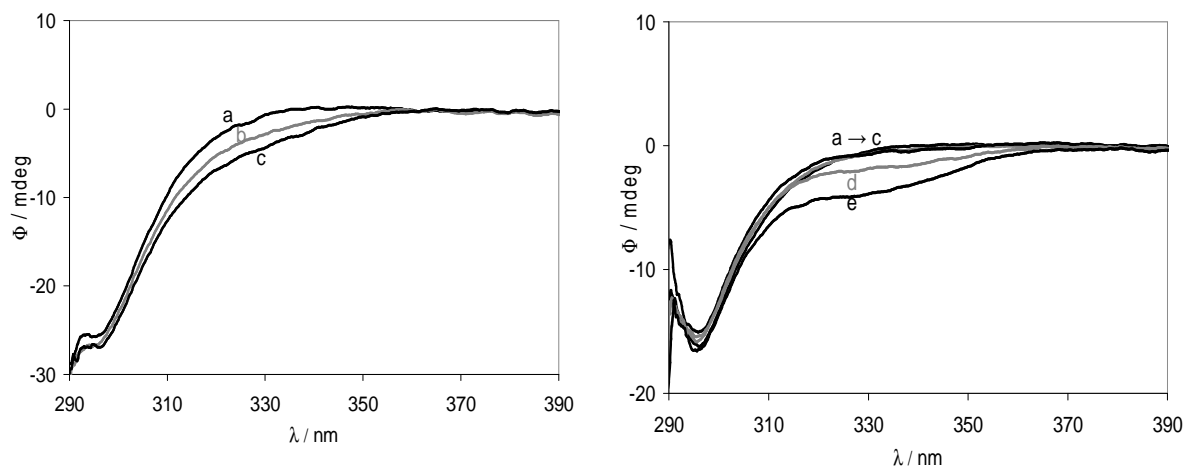


Fig. S-6-8 (A) CD spectra of HSA solution (a, —, $C_{\text{HSA}} = 0.630 \text{ mM}$), and after additions of a solution containing $\text{V}^{\text{IV}}\text{OSO}_4$ and dhp (b, —, $C_{\text{HSA}} = 0.630 \text{ mM}$, $C_{\text{V}} = 80 \mu\text{M}$, $C_{\text{maltol}} = 2 \times C_{\text{V}}$), (c, —, $C_{\text{HSA}} = 0.630 \text{ mM}$, $C_{\text{V}} = 160 \mu\text{M}$, $C_{\text{maltol}} = 2 \times C_{\text{V}}$). (B) CD spectra of a solution containing HSA and apo-hTF (a: $C_{\text{HSA}} = 630 \mu\text{M}$, $C_{\text{hTF}} = 40 \mu\text{M}$) and after additions of a solution containing $\text{V}^{\text{IV}}\text{OSO}_4$ and maltol: (b: $C_{\text{HSA}} = 0.63 \text{ mM}$, $C_{\text{hTF}} = 40 \mu\text{M}$, $C_{\text{V}} = 40 \mu\text{M}$, $C_{\text{maltol}} = 2 \times C_{\text{V}}$); (c: $C_{\text{HSA}} = 0.63 \text{ mM}$, $C_{\text{hTF}} = 40 \mu\text{M}$, $C_{\text{V}} = 80 \mu\text{M}$, $C_{\text{maltol}} = 2 \times C_{\text{V}}$); (d: $C_{\text{HSA}} = 0.63 \text{ mM}$, $C_{\text{hTF}} = 40 \mu\text{M}$, $C_{\text{V}} = 0.16 \text{ mM}$, $C_{\text{maltol}} = 2 \times C_{\text{V}}$); (e: $C_{\text{HSA}} = 0.63 \text{ mM}$, $C_{\text{hTF}} = 40 \mu\text{M}$, $C_{\text{V}} = 0.32 \text{ mM}$, $C_{\text{maltol}} = 2 \times C_{\text{V}}$). All spectra were recorded with a 2 mm optical path quartz cell in HEPES-S buffer at pH 7.4. The CD signals were corrected for the dilution caused by the addition of the solution containing $\text{V}^{\text{IV}}\text{OSO}_4$ and maltol.

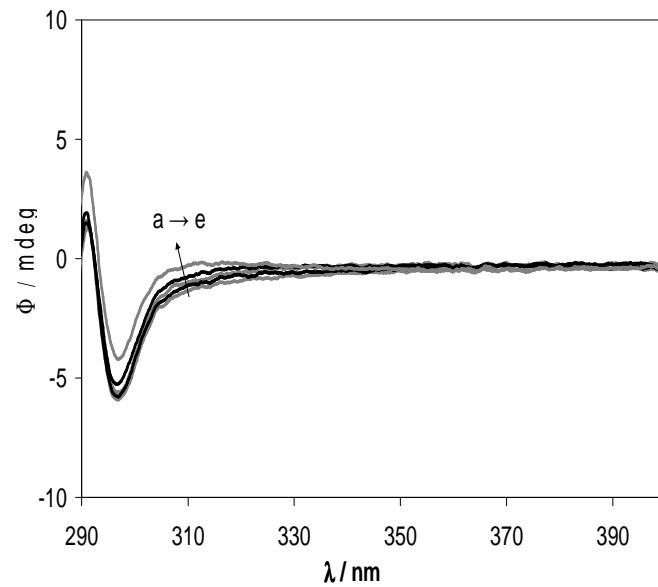


Fig. S-6-9 CD spectra in the 250-400 nm range of solutions containing apo-hTF ($C_{\text{hTF}} = 100 \mu\text{M}$) and after stepwise additions of a solution containing $\text{V}^{\text{IV}}\text{OSO}_4$ and maltol in 1:2 molar ratio in HEPES-CL buffer. (a) apo-hTF; (b) apo-hTF: $\text{V}^{\text{IV}}\text{O}$:maltol = 1:1:2; (c) apo-hTF: $\text{V}^{\text{IV}}\text{O}$:maltol = 1:2:4; (d) apo-hTF: VO : maltol = 1:3:6; (e) apo-hTF: VO : maltol = 1:4:8. The spectra were recorded with a 2 mm optical path quartz cell.

ESI-7 - CD spectra of solutions containing apo-hTF and additions of solutions containing V^VO-mhcpe complexes in the visible range

Fig. S-7-1 depicts CD spectra in the 400-1000 nm range of solutions containing apo-hTF titrated with solutions containing V^{IV}O-mhcpe complexes.

Quite similar CD spectra and trends were found when adding solutions containing apo-hTF and V^{IV}OSO₄ titrated with mhcep (see Fig. 14 in the main text) pH 7.4. All observations suggest the formation of complexes with stoichiometries (V^{IV}O)₁(hTF)(mhcep)₁, (V^{IV}O)₂(hTF)(mhcep)₁ and (V^{IV}O)₂(hTF)(mhcep)₂.

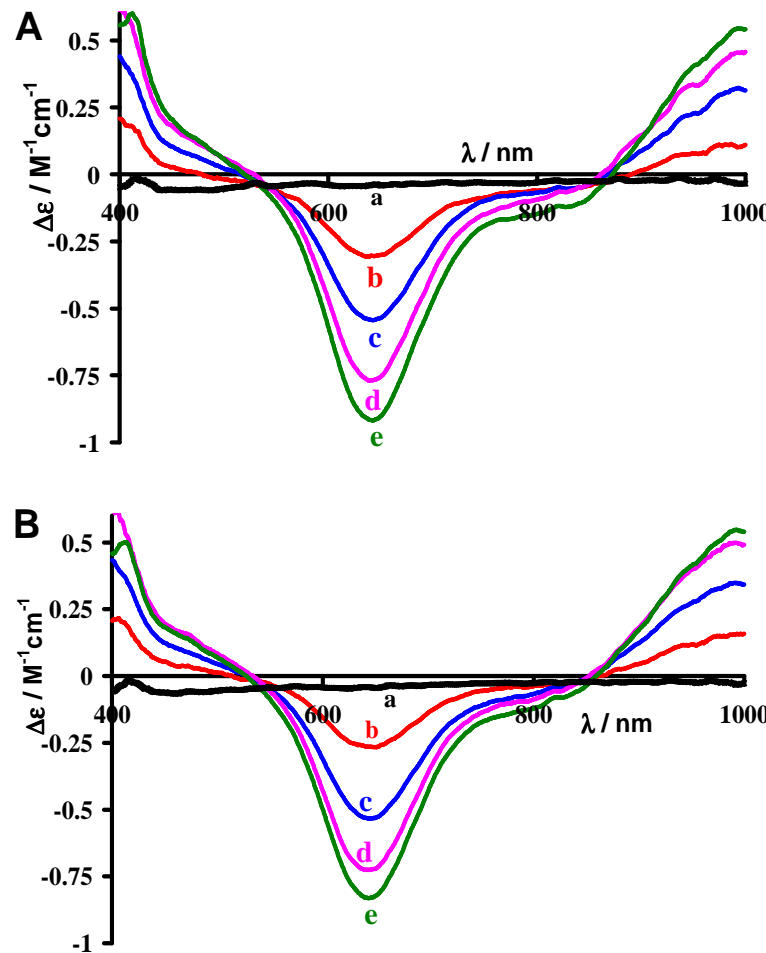


Fig. S-7-1 CD spectra in the 400-1000 nm range of solutions in HEPES-S buffer at pH 7.4 containing (A) apo-hTF and V^{IV}O-mhcpe (1:1) ($C_{\text{HTF}} = 750 \mu\text{M}$) (a) apo-hTF; (b) apo-hTF:V^{IV}O:mhcpe = 1:0.5:0.5; (c) apo-hTF:V^{IV}O:mhcpe = 1:1:1; (d) apo-hTF:VO:mhcpe = 1:1.5:1.5; (e) apo-hTF:VO:mhcpe = 1:2:2, and (B) apo-hTF and V^{IV}O-mhcpe (1:2) ($C_{\text{HTF}} = 750 \mu\text{M}$) (a) apo-hTF; (b) apo-hTF:V^{IV}O:mhcpe = 1:0.5:1; (c) apo-hTF:V^{IV}O:mhcpe = 1:1:2; (d) apo-hTF:VO:mhcpe = 1:1.5:3; (e) apo-hTF:VO:mhcpe = 1:2:4. The spectra were recorded with a 50 mm optical path quartz cell.

Figure S-7-2 depict CD spectra in the 400-1000 nm range of solutions containing apo-hTF titrated with solutions containing sodium vanadate and mhcpe. No CD signal is detected for $\lambda > 500$ nm, this indicating that no V^{IV} -species are formed (as no CD due to d-d bands are recorded), and no CD charge transfer band is detected in this wavelength range.

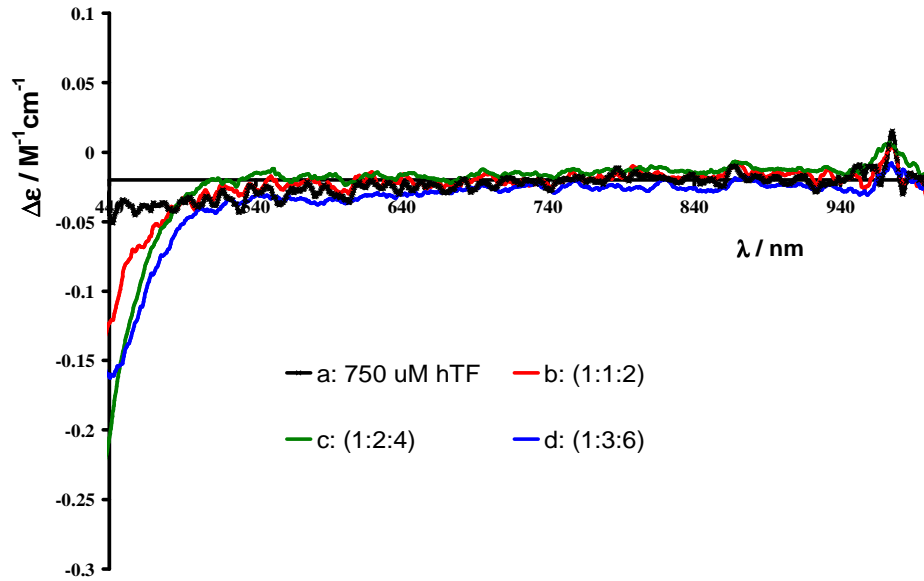


Fig. S-7-2 CD spectra in the 400-1000 nm range of solutions in Hepes-CL buffer at pH 7.4 containing apo-hTF (a) $C_{\text{hTF}} = 0.750 \text{ mM}$ and after addition of a solution containing sodium vanadate and of a solution of mhcpe. The molar ratios are indicated. The spectra were recorded with a 50 mm optical path quartz cell.

The peaks detected in the ^{51}V NMR spectra of solutions corresponding to the solutions of Figure S-7-2 vary according to the particular solution considered:

- Solution of the dark-blue spectrum (hTF: V^V :mhcpe molar ratios of 1:1:2): only a peak at *ca.* -532 ppm, corresponding to the $(\text{hTF})_n V^V$ complex, is detected.
- Solution of the green spectrum (hTF: V^V :mhcpe molar ratios of 1:2:4): only two equally intense peaks are detected, one at *ca.* -531/-532 ppm corresponding to the $(\text{hTF})_n V^V$ complex, and one at *ca.* -558 ppm corresponding to free vanadate (V_1).
- Solution of the light-blue spectrum (hTF: V^V :mhcpe molar ratios of 1:3:6): three peaks are detected; two are the same as in (b) -532 ppm (19%), -558 ppm (70%, probably monovanadate, V_1), and one at *ca.* -572 ppm (11%) which may correspond to a divanadate species (V_2).
- Solution of the light-blue spectrum (hTF: V^V :mhcpe molar ratios of 1:4:8): four peaks are detected; two are the same as in (b,c) -532 ppm (8%), -558 ppm (64%), and one at *ca.* -572 ppm (22%) corresponding to a V^V -mhcpe complex,⁴² and one at -513 ppm (6%), which probably corresponds to $\text{VO}_2(\text{mhcpe})$.⁴²

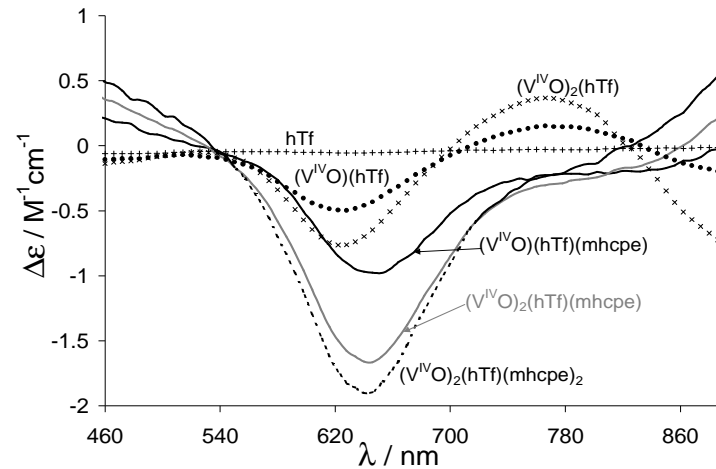


Fig. S-7-3 Calculated visible CD spectra of each individual species formed in the $[(V^{IV}O)_p(hTF)_q(mhcpe)_r]$ system, using the PSEQUAD program⁵⁹ with the conditional formation constants given in Table 4. The low concentration of the $[(V^{IV}O)_2(hTF)(mhcpe)]$ species in the experimental conditions used limits the accuracy of the calculated spectra.

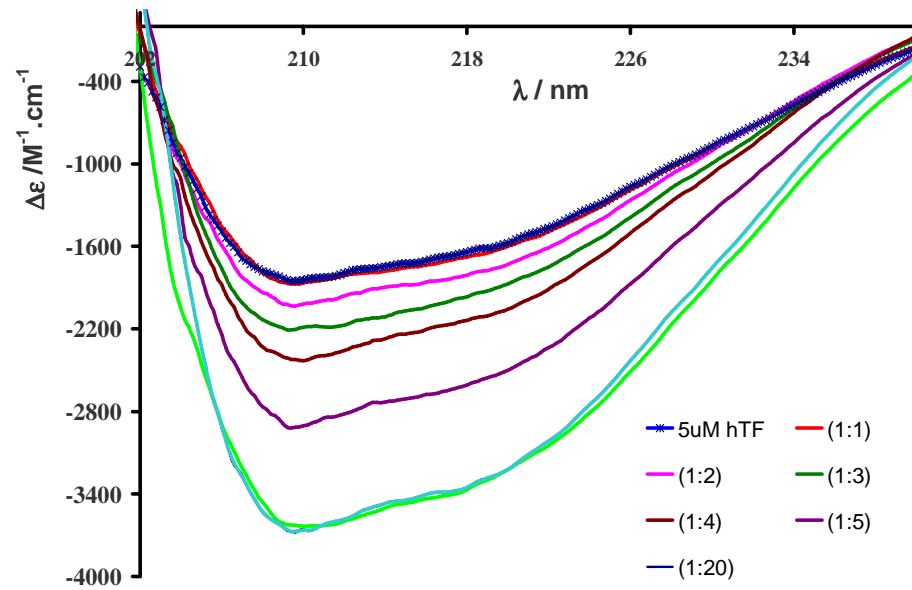


Fig. S-7-4 CD spectra of hTF (5 μM) solution (xxxx) and after stepwise additions of a solution containing $V^{IV}\text{OSO}_4$ in a PBS buffer at pH 7.4. The hTF: $V^{IV}\text{OSO}_4$ molar ratio are indicated. The spectra were recorded with a 1 mm optical path quartz cell.

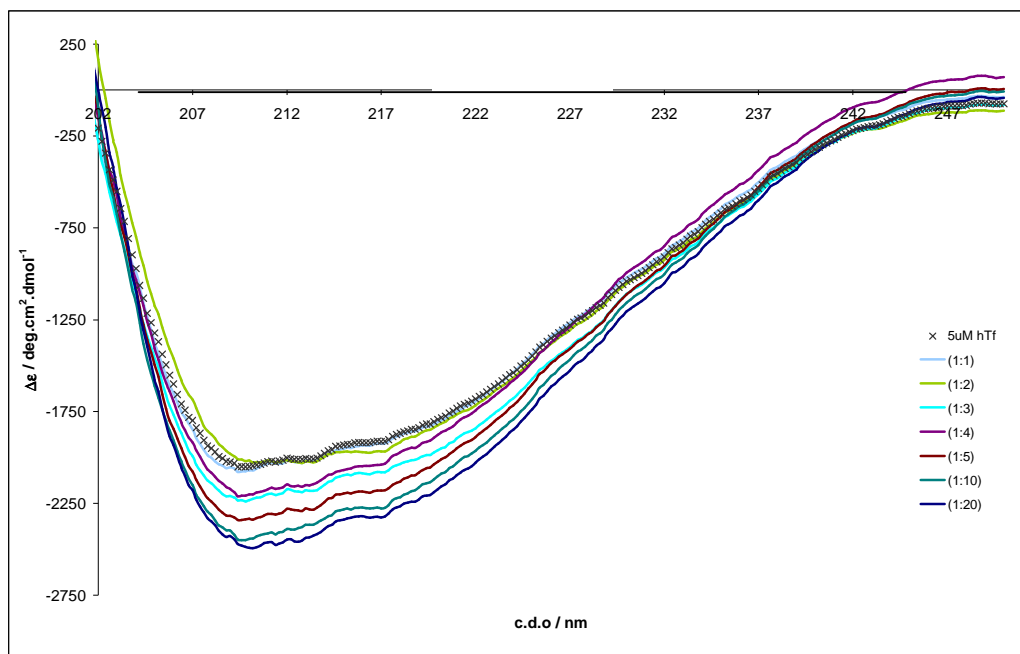


Fig. S-7-5 CD spectra of hTF (5 μM) solution (xxxx) and after stepwise additions of a solution containing V^{IV}OSO₄ and mhcpe in a 1:2 molar ratio in a PBS buffer at pH 7.4. The hTF:V^{IV}OSO₄:mhcpe molar ratios are indicated. The spectra were recorded with a 1 mm optical path quartz cell.

SI-8 - Spectra of solutions containing apo-hTF, V^{IV}OSO₄, Fe^{III} and mhcppe

In solutions containing V^{IV}O²⁺ and hTF in conditions where there are enough free available sites for the binding of all V^{IV}O²⁺ present, we observed that this metal ion is more easily oxidized to V^V than in the absence of Fe^{III}. A similar effect is observed in solutions also containing mhcppe, maltol or dhp. Fig. S-8-1 includes CD spectra of solutions containing apo-hTF (spectrum 1) and after stepwise additions of a solution containing V^{IV}O²⁺ and mhcppe with a 1:2 molar ratio (spectra 2-4). These spectra are similar to those presented in Fig. 9 and the solution of spectrum 4 contains enough V^{IV} to bind to 70% of the hTF Fe^{III}-binding sites. Upon addition of a solution containing an amount of Fe^{III} equivalent to 30% of the hTF Fe^{III}-binding sites the ICD bands in the 500-1000 nm range, assigned to V^{IV}O d-d transitions, decrease continuously with time due to the relatively fast oxidation of V^{IV}O- to V^V-species (Fig. S-8-1). This relatively fast oxidation occurs despite the hTF present in solution contains enough binding sites to bind all V^{IV}O and Fe^{III} added.

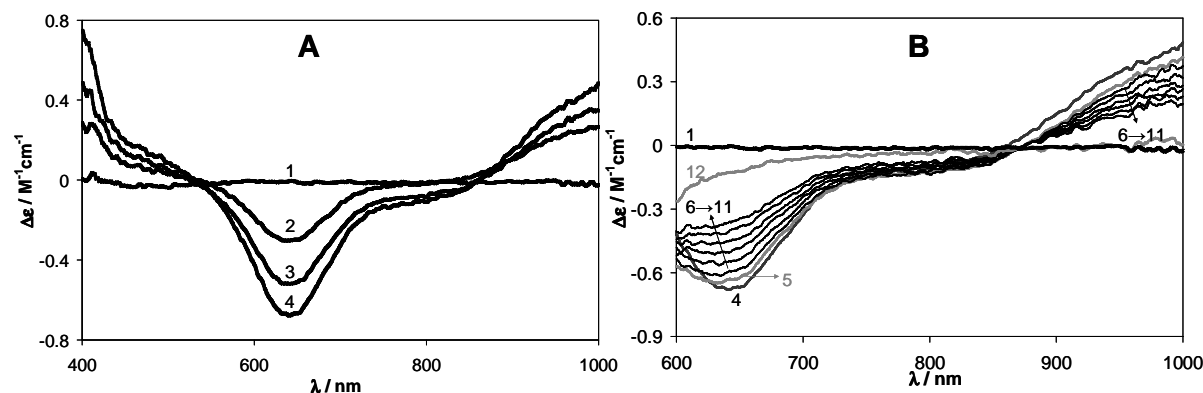


Fig. S-8-1 (A) CD spectra in the 400-1000 nm range of solutions containing (A) (1) apo-hTF ($C_{\text{hTF}} = 0.750 \text{ mM}$) (2) apo-hTF, V^{IV}OSO₄ and mhcppe ($C_{\text{hTF}} \approx 0.75 \text{ mM}$, $C_{\text{VO}} = 0.6 \times C_{\text{hTF}}$, $C_{\text{mhcppe}} = 1.2 \times C_{\text{hTF}}$); (3) apo-hTF, V^{IV}OSO₄ and mhcppe ($C_{\text{hTF}} \approx 0.75 \text{ mM}$, $C_{\text{VO}} = C_{\text{hTF}}$, $C_{\text{mhcppe}} = 2.0 \times C_{\text{hTF}}$) and (4) apo-hTF, V^{IV}OSO₄ and mhcppe ($C_{\text{hTF}} \approx 0.75 \text{ mM}$, $C_{\text{VO}} = 1.4 \times C_{\text{hTF}}$, $C_{\text{mhcppe}} = 2.8 \times C_{\text{hTF}}$). (B) (5) Spectrum recorded after addition, to the solution of spectrum (4), of a Fe^{III} solution such that the final concentrations are $C_{\text{hTF}} \approx 0.75 \text{ mM}$, $C_{\text{VO}} = 1.4 \times C_{\text{hTF}}$, $C_{\text{mhcppe}} = 2.8 \times C_{\text{hTF}}$, $C_{\text{Fe}} = 0.6 \times C_{\text{hTF}}$, and (6-11): spectra of this solution recorded with 10 min time intervals without removing the sample from the cell. All spectra were recorded with a 50 mm optical path quartz cell (see ESI-4). All manipulations were done in an inert (argon) atmosphere (except the preparation of the Fe^{III} solution). At the end of the measurement of spectrum 11 (time = 60 min after spectrum 5), the 50 mm quartz cell was removed from the sample compartment, the stopper of the cell was removed, the solution allowed to air oxidize and spectrum 12 was recorded 20 min later.

Fig. S-8-2 includes several EPR spectra comparing the V^{IV}O-signals measured in several distinct conditions. In all figures presented in this section the hTF concentration is *ca.* 0.75 mM and pH = 7.4 (Hepes-S buffer). The concentrations of all other reagents can be obtained from the molar ratios given for each spectrum presented.

Upon addition of Fe^{III} to a solution containing apo-hTF and V^{IV}O²⁺ (1:2), the V^{IV}O-EPR spectrum changes significantly: (i) the global intensity decreases, (ii) the relative intensity of the C-terminal site (the B component in the V^{IV}O-EPR spectrum), which binds Fe^{III} more strongly decreases drastically, and (iii) a very slight decrease in the A_z value is noticed.

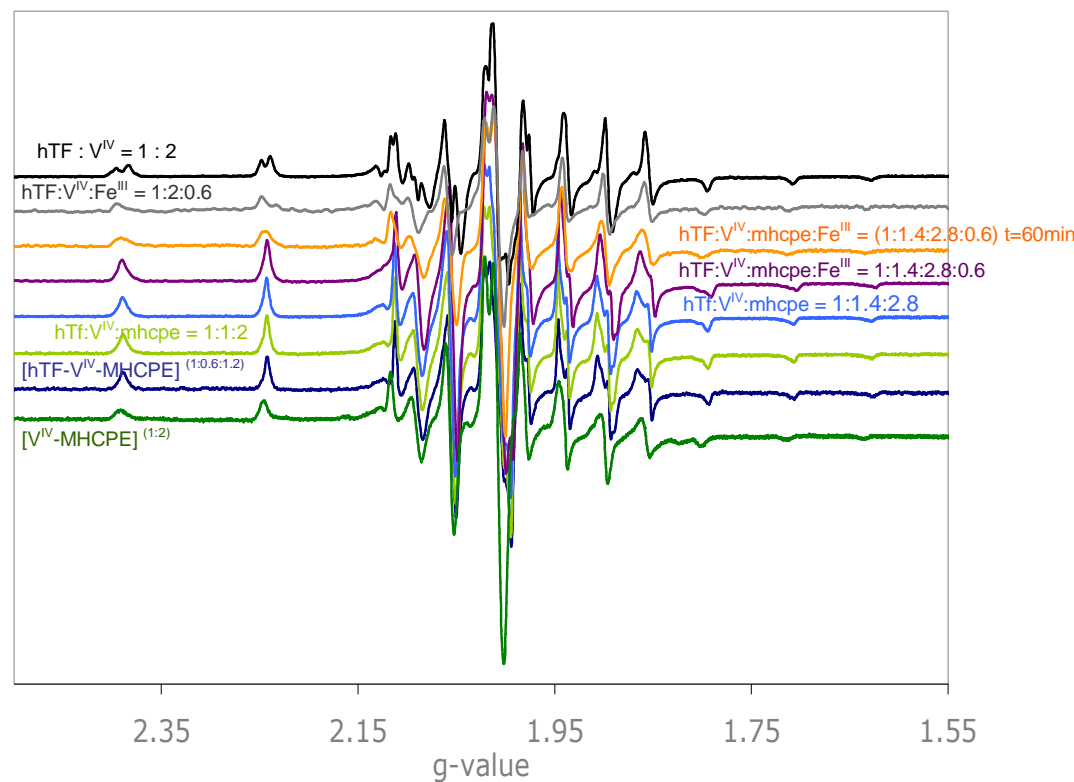


Fig. S-8-2 - First derivative EPR spectra of frozen solutions containing the reagents indicated for each colored spectrum in HEPES-S buffer of pH = 7.4. The low and high field ranges for these spectra are presented amplified in Fig. S-8-3.

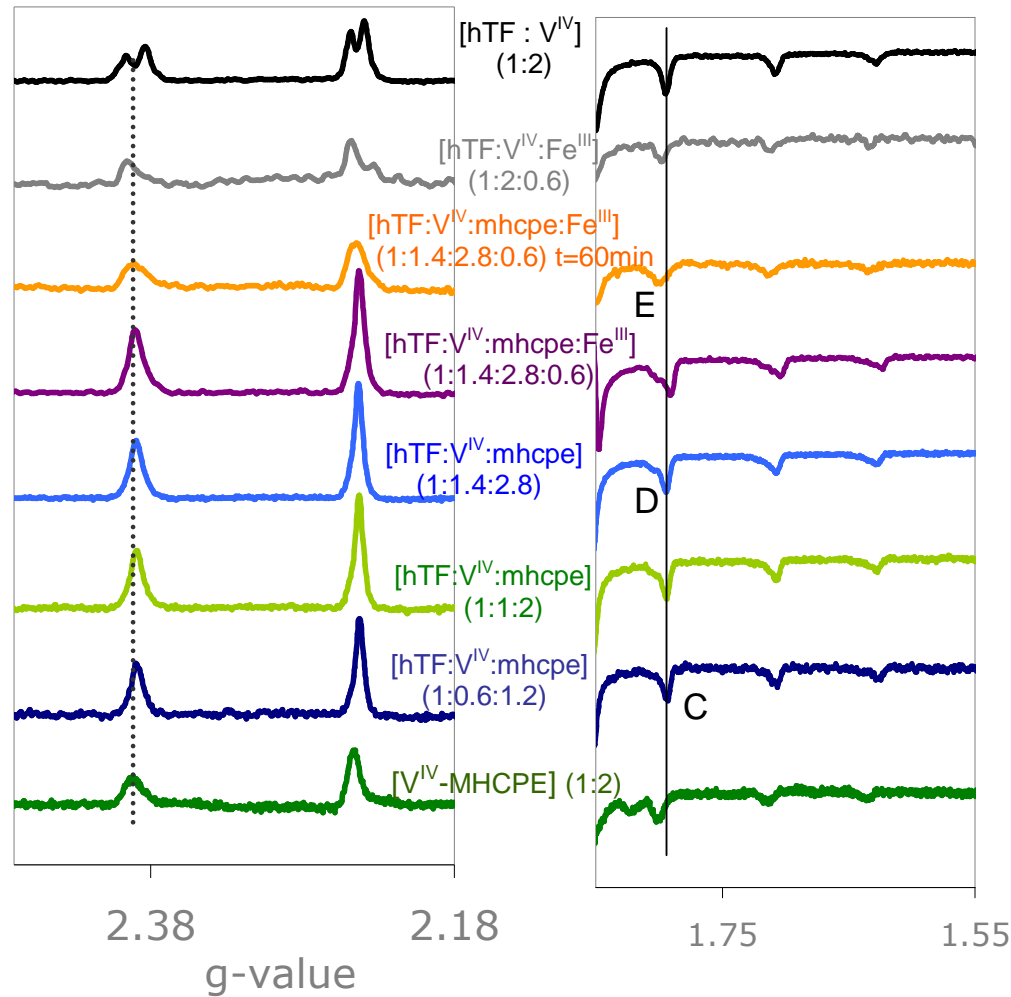


Fig. S-8-3 – Amplification of the low and high field ranges first derivative EPR spectra of frozen solutions containing the reagents indicated for each colored spectrum in Hepes-S buffer of pH = 7.4. These spectra correspond to those presented in Fig. S-8-1.

Species	g_z	A_z	Ref
A	1.938	168.0	77
B	1.938	170.0	77
I C	1.941	170.4	This work
II D	1.946	166.5	This work
III E	1.941	168.2	This work

Fig. SI-8-4 depicts a ^{51}V NMR spectrum of the solution which originated CD spectrum 12 of Fig. S-8-1, *i.e.* *ca.* 1 h after the addition of the Fe^{III} solution to the solution containing hTF (*ca.* 0.75 mM), $\text{V}^{\text{IV}}\text{OSO}_4$, mhcppe and Fe^{III} in the 1:1.4:2.8:0.6 molar ratio, and more 20 min after removing the stopper of the quartz cell. No signal corresponding to any hTF- V^{V} -mhcppe species was detected in this or in other experiments.

750 μM hTF-V4mhcppe-Fe (1:1.4:2.8:0.6) (Hepes-S)

[hTF- V^{IV} -MHCPE- Fe^{III}] (1:1.4:2.8:0.6) $t=60\text{min}$

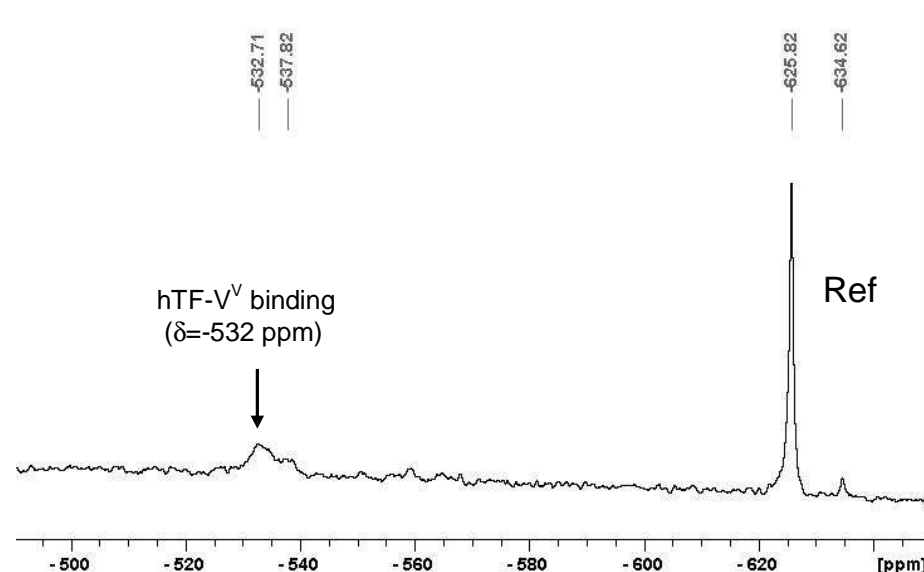


Fig. S-8-4 ^{51}V NMR spectrum corresponding to CD spectrum 12 of Fig. Tf-11 of the text, therefore it contains: hTF (*ca.* 0.75 mM), $\text{V}^{\text{IV}}\text{O}^{2+}$ (*ca.* 1.05 mM), mhcppe (*ca.* 2.10 mM) and Fe^{III} (*ca.* 0.45 mM) in Hepes-S buffer at pH = 7.4. The peak at *ca.* -532 ppm corresponds to the V^{V} -hTF complex, and the peak at *ca.* -538 ppm corresponds to a V^{V} -mhcppe complex. The reference shown is $[\text{V}^{\text{V}}\text{O}(\text{O})_2]$. The reference was measured against neat $\text{V}^{\text{V}}\text{OCl}_3$ ($\delta=0$).

Experiment in which the amount of Fe^{III} added will bind to ~30% of the iron binding sites of hTF, and there are more than enough sites in hTF to bind all V^{IV}O present. Of a total of 2 equivalents of binding sites, only a maximum of 1.6 equivalents may be occupied by Fe^{III} and V^{IV}O. Thus there are still free binding sites not bound to any metal ion:

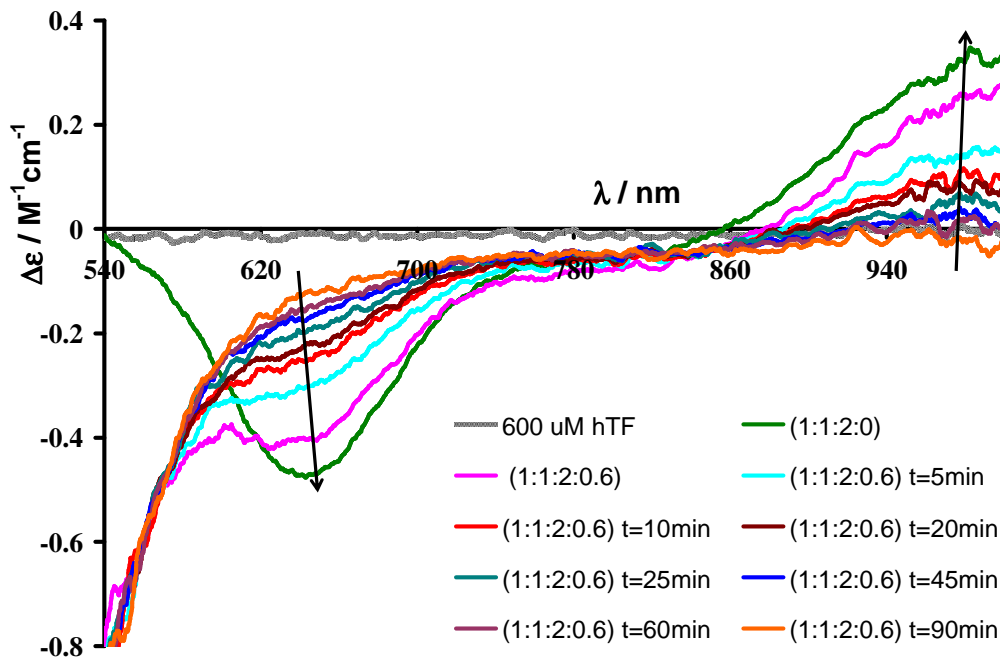


Fig. S-8-5 CD spectra in the 400-1000 nm range of solutions containing apo-hTF in Hepes-CL buffer at pH 7.4 ($C_{hTF} = 0.600$ mM) and (2, green) apo-hTF after addition of a solution containing V^{IV}OSO₄ and mhcpe (1:2 molar ratio) so that: $C_{hTF} \approx 0.60$ mM, $C_{VO} = C_{hTF} \approx 0.60$ mM and $C_{mhcpe} = 2 \times C_{VO} \approx 1.20$ mM and (3, pink) the same solution after addition of a Fe^{III} solution such that $C_{Fe} = 0.6 \times C_{hTF} \approx 0.36$ mM. Thus not all iron binding sites of hTF may be bound to metal ions, as the Fe^{III} present corresponds to 30 % and V^{IV}O so 50 % of these sites. The molar ratios: hTF:V^{IV}O;mhcpe:Fe are indicated. Several CD spectra of this solution last solution also containing Fe^{III} were measured with time (indicated) without removing the sample from the cell. All spectra were recorded with a 50 mm optical path quartz cell (see ESI-4). All manipulations were done in an inert (argon) atmosphere (except the preparation of the Fe^{III} solution). A peak at ca. -531 ppm was detected in the ⁵¹V NMR spectrum of the solution 60 min. after addition of Fe^{III}, but not in the solution immediately after adding Fe^{III}.

Experiment in which the amount of Fe^{III} added will bind to ~30% of the iron binding sites of hTF, and there are just enough binding sites for the V^{IV}O centres to bind. Of a total of 2 equivalents of binding sites, only a maximum of 0.6 equivalents are occupied by Fe^{III}, and the remaining 1.4 equivalents may be bound to the V^{IV}O centres present in solution. Thus there are still free binding sites not bound to any metal ion

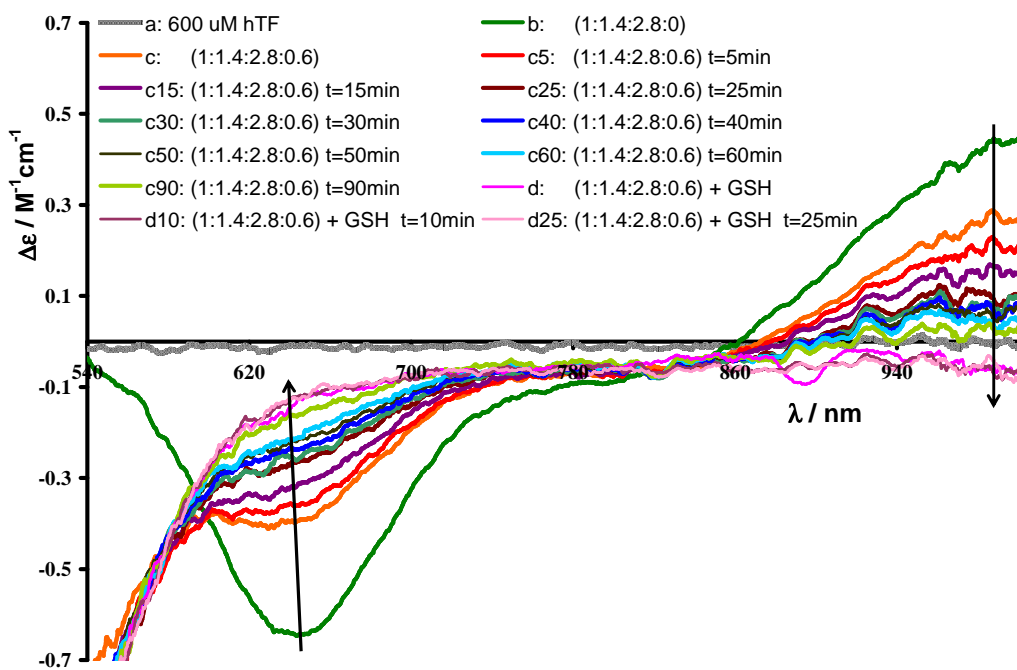


Fig. S-8-6 CD spectra in the 400-1000 nm range of solutions containing apo-hTF in Hepes-CL buffer at pH 7.4 ($C_{\text{hTF}} = 0.600 \text{ mM}$) and (b) apo-hTF after addition of a solution containing V^{IV}OSO₄ and mhcpe so that: $C_{\text{hTF}} \approx 0.60 \text{ mM}$, $C_{\text{VO}} = 1.20 \text{ mM}$ and $C_{\text{mhcpe}} = 2.8 \text{ mM}$; (c) the same solution after addition of a Fe^{III} solution such that the final concentrations are $C_{\text{hTF}} \approx 0.60 \text{ mM}$ ($C_{\text{Fe}} = 0.6 \times C_{\text{hTF}}$); thus the amount of Fe^{III} and V^{IV}O added correspond exactly to the amount needed to saturate the iron binding sites of hTF. The molar ratios hTF:V^{IV}O:mhcpe:Fe are indicated. Several CD spectra of this solution were measured with time (indicated) without removing the sample from the cell. (d) After the CD spectrum corresponding to 90 minutes after addition of Fe^{III} was recorded(c90), an excess of glutathione (GSH) was added to the solution. No changes were noticed in the CD spectra recorded, thus no reduction to V^{IV} of any V^V-species formed after addition of Fe^{III} is detected by CD. All spectra were recorded with a 50 mm optical path quartz cell (see ESI-4). All manipulations were done in an inert (argon) atmosphere (except the preparation of the Fe^{III} solution). A peak at ca. -531 ppm was detected in the ⁵¹V NMR spectrum of the solution 60 min. after addition of Fe^{III}, but not in the solution immediately after adding Fe^{III}.

The EPR spectra depicted in Figs. S-8-6A and –B also do not show significant changes after addition of GSH.

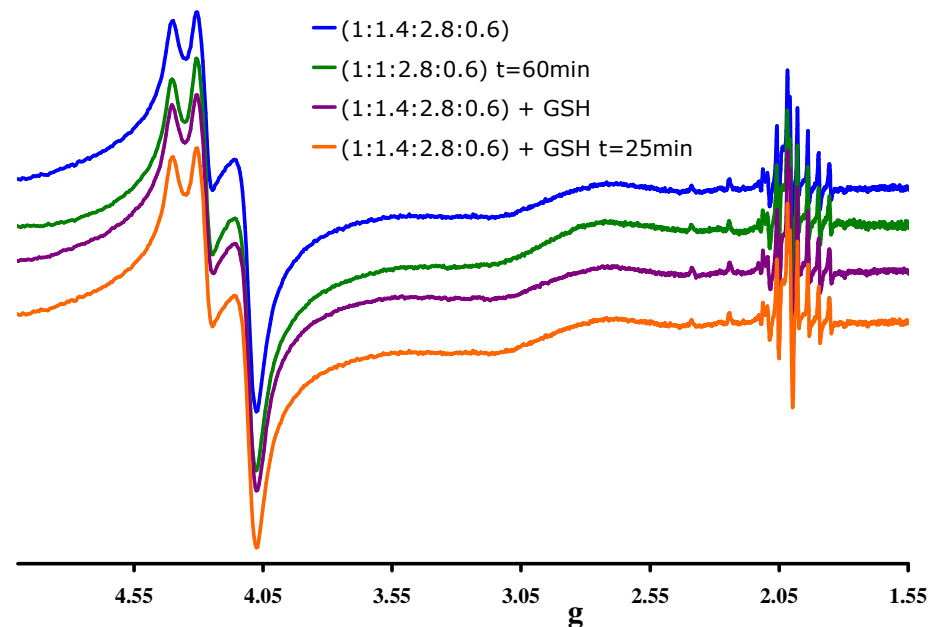


Fig. S-8-7A First derivative EPR spectra of solutions containing (1) apo-hTF, V^{IV}OSO₄, mhcppe and Fe^{III} (molar ratios: 1 : 1.4 : 2.8 : 0.6) in Hepes-CL buffer at pH 7.4 ($C_{\text{hTF}} = 0.600$ mM); (2) of the same solution after ca. 60 min.; (3) the same solution (after ca. 90 min.) and upon addition of an excess of GSH; (4) the same solution of (3) after 25 min. These spectra correspond to the solutions used to measure some of the CD spectra included in Fig. S-8-5.

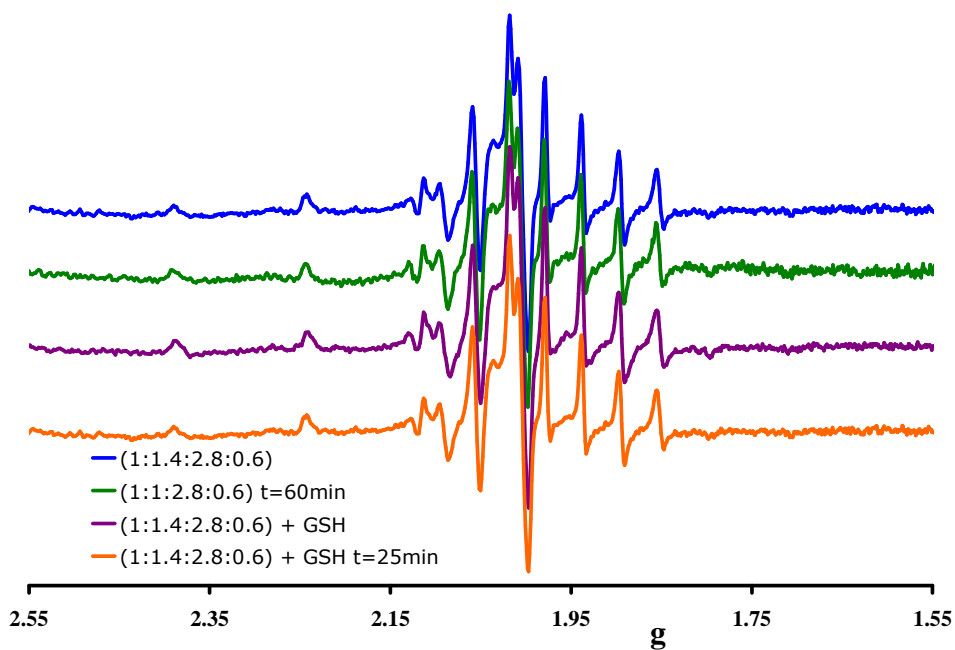


Fig. S-8-7B First derivative EPR spectra of solutions containing (1) apo-hTF, $\text{V}^{\text{IV}}\text{OSO}_4$, mhcp and Fe^{III} (molar ratios: 1 : 1.4 : 2.8 : 0.6) in Hepes-CL buffer at pH 7.4 ($C_{\text{hTF}} = 0.600 \text{ mM}$); (2) of the same solution after ca. 60 min.; (3) the same solution (after ca. 90 min.) and upon addition of an excess of GSH; (4) the same solution of (3) after 25 min. These spectra are those of Fig. S-8-6A but showing only the $g = 2.05 \pm 0.5$ range to depict only the signals corresponding to the $\text{V}^{\text{IV}}\text{O}$ -species.

SI-9

Circular dichroism spectra of solutions containing HSA, V^{IV}OSO₄ and mhcpe – far UV range

Figure S-9-1 includes CD spectra in the 200-250 nm range of solutions containing HSA, V^{IV}OSO₄ and mhcpe. Adding up to a molar ratio of V^{IV}O:HSA of 1, the CD spectra practically do not change, but upon further stepwise additions of V^{IV}O(mhcpe)₂, up to a molar ratio of 20 (HSA: V^{IV}O(mhcpe)₂), the $\Delta\epsilon$ values change, but not the global pattern of the CD spectra. Therefore, upon addition of complex, there may be some conformational changes of the protein, but not very extensive (see text).

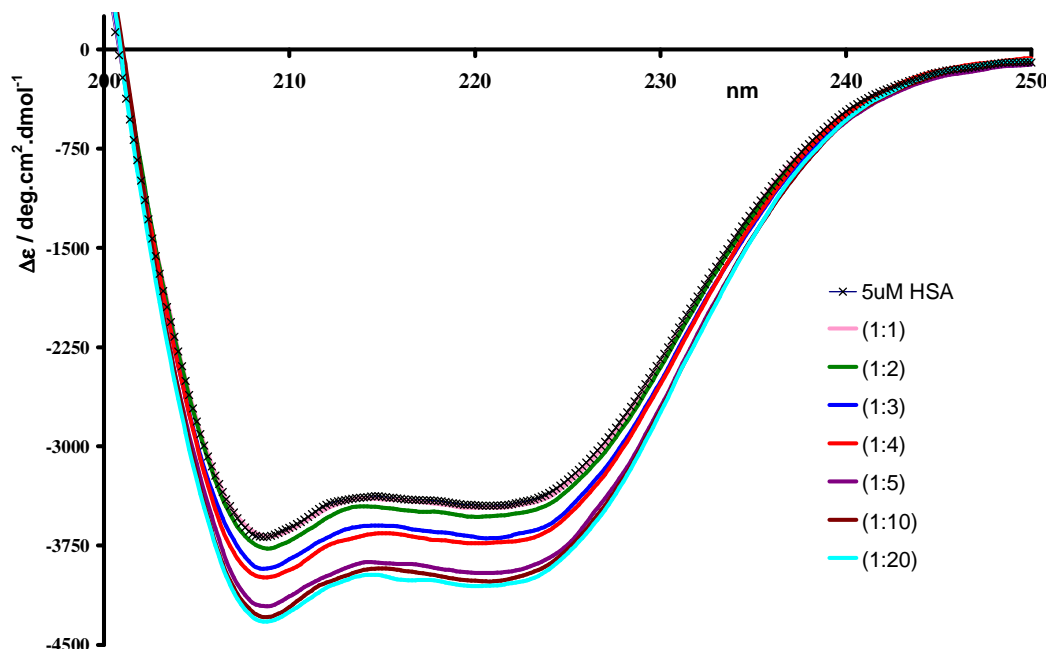
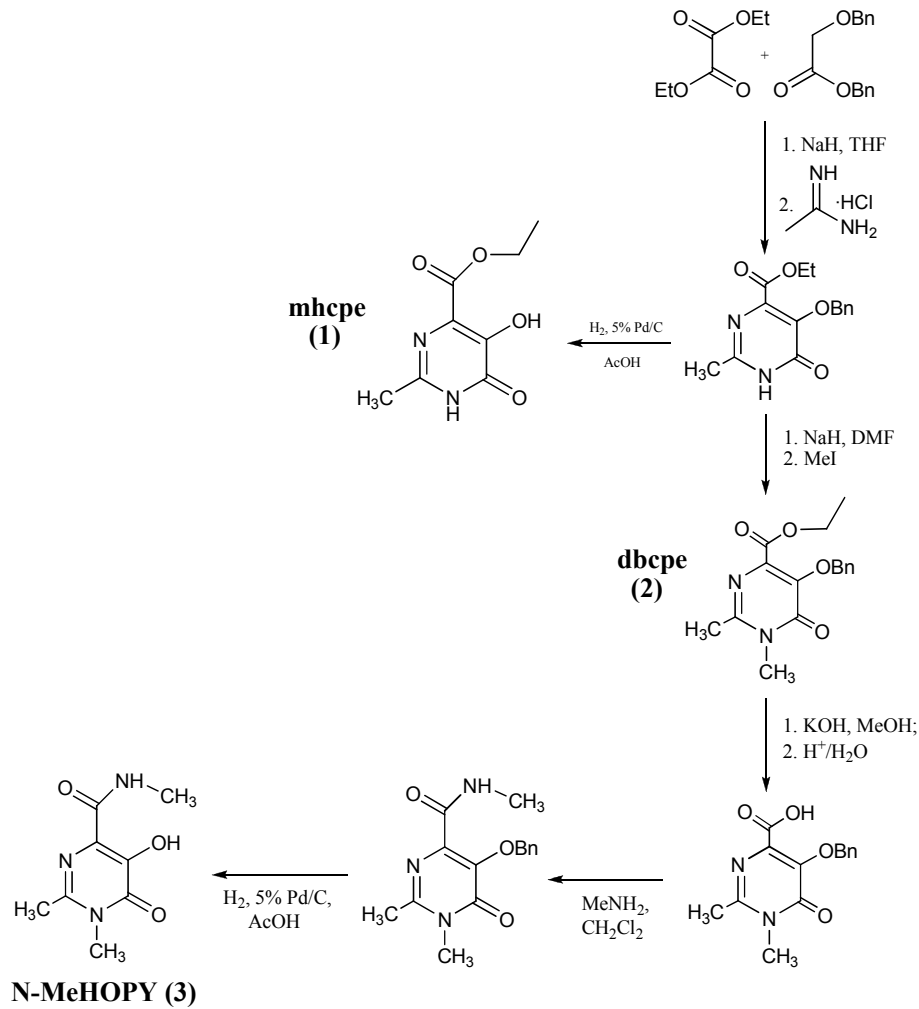


Figure SI-9-1. – CD spectra of HSA (5 μM) solution (xxxx) and after stepwise additions of a solution containing V^{IV}OSO₄ and mhcpe in a 1:2 molar ratio in a PBS buffer at pH 7.4. The HSA:V^{IV}O(mhcpe)₂ molar ratios are indicated. The spectra were recorded with a 1 mm optical path quartz cell.

ESI – 10 - Synthesis of mhcp (1), dbcpe (2), N-MeHOPY (3) and X-ray diffraction data

The pyridiminone mhcp (1) was prepared as outlined in Scheme S-9-1 (see also experimental section), while dbcpe (2) was synthesized from one of the intermediates and N-MeHOPY (3) was obtained from 2, as also indicated in Scheme S-9-1.



Scheme S-10-1 Outline of the main steps for the synthesis of **1** (2-methyl-3H-5-hydroxy-6-carboxy-4-pyrimidinone ethyl ester, mhcp), **2** (2,3-dimethyl-5-benzyloxy-6-carboxy-4-pyrimidinone ethyl ester, dbcpe) and **3** (N-methyl-2,3-dimethyl-5-hydroxy-6-carboxyamido-4-pyrimidinone, N-MeHOPY). ⁴¹

These compounds were characterized by ¹H and ¹³C NMR, mass spectrometry and by single crystal x-ray diffraction, and their purity was confirmed by elemental analysis.

X-Ray crystal structure determinations. Three-dimensional X-ray data were collected on a Bruker SMART 1000 CCD diffractometer using a graphite monochromator and Mo- K_{α} radiation ($\lambda = 0.71073 \text{ \AA}$) by the $\phi\omega$ scan method. Data was collected at room temperature. Reflections were measured from a hemisphere of data collected of frames each covering 0.3 degrees in ω . Of the 4415 for **1**, 8387 for **2** and 5823 for **3** reflections measured, all of which were corrected for Lorentz and polarization effects, and for absorption by semi-empirical methods based on symmetry-equivalent and repeated reflections, 985 for **1**, 1502 for **2** and 1870 for **3** independent reflections exceeded the significance level $|F|/\sigma(|F|) > 4.0$. Complex scattering factors were taken from the program package SHELXTL.^{88,89} The structure was solved by direct methods and refined by full-matrix least-squares methods on F^2 . In **1**, the hydrogen atoms were included in calculated positions and refined in riding mode except the hydrogen atom H(2O), which was located in difference Fourier map and freely refined; in **2**, all of them were included in calculated positions; in **3** all of them were located in difference Fourier map and freely refined. Refinement converged with allowance for thermal anisotropy of all non-hydrogen atoms. A weighting scheme $w = 1/[\sigma^2(F_o^2) + (0.113100P)^2]$ for **1**, $w = 1/[\sigma^2(F_o^2) + (0.108600P)^2 + 0.019500P]$ for **2** and $w = 1/[\sigma^2(F_o^2) + (0.056900P)^2 + 0.867500P]$ for **3**, where $P = (|F_o|^2 + 2|F_c|^2)/3$, were used in the latter stages of refinement. A final difference Fourier map showed no residual density outside: 0.305 and $-0.298 \text{ e}\cdot\text{\AA}^{-3}$ in **1**, 0.222 and $-0.236 \text{ e}\cdot\text{\AA}^{-3}$ in **2**, 0.340 and $-0.176 \text{ e}\cdot\text{\AA}^{-3}$ in **3**.

Table S-10-1 Crystal data and structure refinement for mhcp (1), dbcpe (2) and N-MeHOPY (3).

A: Data for mhcp (1)

Identification code	mhcp (1)		
Formula	C8 H10 N2 O4		
Formula weight	198.18		
Temperature	298(2) K		
Wavelength	0.71073 Å		
Crystal system	Monoclinic		
Space group	C2/c		
Unit cell dimensions	a = 26.412(19) Å	α = 90°.	b = 4.442(3) Å
	c = 15.994(11) Å	β = 113.034(12)°.	γ = 90°.
Volume	1727(2) Å ³		
Z	8		
Density (calculated)	1.525 Mg/m ³		
Absorption coefficient	0.124 mm ⁻¹		
F(000)	832		
Crystal size	0.48 x 0.13 x 0.06 mm ³		
Theta range for data collection	1.68 to 26.38°.		
Index ranges	-32<=h<=30, -5<=k<=5, -19<=l<=11		
Reflections collected	4415		
Independent reflections	1751 [R(int) = 0.0585]		
Completeness to theta = 26.38°	98.6 %		
Absorption correction	Semi-empirical from equivalents		
Max. and min. transmission	0.9926 and 0.9429		
Refinement method	Full-matrix least-squares on F ²		
Data / restraints / parameters	1751 / 0 / 133		
Goodness-of-fit on F ²	0.937		
Final R indices [I>2sigma(I)]	R1 = 0.0562, wR2 = 0.1439		
R indices (all data)	R1 = 0.1110, wR2 = 0.1892		
Largest diff. peak and hole	0.305 and -0.296 e.Å ⁻³		

B: Data for dbcpe (2):

Identification code	dbcpe (2)
Formula	C ₁₆ H ₁₈ N ₂ O ₄
Formula weight	302.32
Temperature	298(2) K
Wavelength	0.71073 Å
Crystal system	Monoclinic
Space group	P2(1)/c
Unit cell dimensions	a = 10.6417(19) Å α = 90°. b = 8.0586(15) Å β = 96.853(4)°. c = 18.579(3) Å γ = 90°.
Volume	1581.9(5) Å ³
Z	4
Density (calculated)	1.269 Mg/m ³
Absorption coefficient	0.092 mm ⁻¹
F(000)	640
Crystal size	0.50 x 0.10 x 0.06 mm ³
Theta range for data collection	1.93 to 25.68°.
Index ranges	-12<=h<=12, -7<=k<=9, -22<=l<=20
Reflections collected	8387
Independent reflections	3005 [R(int) = 0.0377]
Completeness to theta = 25.68°	99.9 %
Absorption correction	Semi-empirical
Max. and min. transmission	0.9945 and 0.9554
Refinement method	Full-matrix least-squares on F ²
Data / restraints / parameters	3005 / 0 / 199
Goodness-of-fit on F ²	1.042
Final R indices [I>2sigma(I)]	R1 = 0.0564, wR2 = 0.1630
R indices (all data)	R1 = 0.1298, wR2 = 0.2078
Largest diff. peak and hole	0.222 and -0.236 e.Å ⁻³

C: Data for N-MeHOPY (3):

Identification code	N-MeHOPY(3)
Formula	C ₈ H ₁₁ N ₃ O ₃
Formula weight	197.20
Temperature	298(2) K
Wavelength	0.71073 Å
Crystal system	Monoclinic
Space group	C2/c
Unit cell dimensions	a = 16.600(2) Å α = 90°. b = 7.8212(11) Å β = 105.112(2)°. c = 14.414(2) Å γ = 90°.
Volume	1806.7(4) Å ³
Z	8
Density (calculated)	1.450 Mg/m ³
Absorption coefficient	0.113 mm ⁻¹
F(000)	832
Crystal size	0.50 x 0.32 x 0.15 mm ³
Theta range for data collection	2.54 to 28.72°
Index ranges	-19≤h≤21, -10≤k≤6, -19≤l≤14
Reflections collected	5823
Independent reflections	2192 [R(int) = 0.0209]
Completeness to theta = 28.72°	93.0 %
Max. and min. transmission	0.9833 and 0.9457
Refinement method	Full-matrix least-squares on F ²
Data / restraints / parameters	2192 / 0 / 171
Goodness-of-fit on F ²	1.050
Final R indices [I>2sigma(I)]	R1 = 0.0402, wR2 = 0.1056
R indices (all data)	R1 = 0.0472, wR2 = 0.1110
Largest diff. peak and hole	0.340 and -0.176 e.Å ⁻³

In the crystals of mhcppe the N(1) atom is protonated and N(2) is not protonated. Atoms O(2)-H … O(3) are involved in intramolecular hydrogen bonds [O(2)-O(3) 2.628(3) Å, H(2O)-O(3) 1.91(4) Å and O(2)-H(2O)-O(3) 141(4)°] and each two molecules form a H-bonded dimer in the solid-state. Other intermolecular H-bonds are also observed (see text).

The solid state structure of dbcpe has no hydrogen bond interactions. In the crystal of N-MeHOPY the hydrogen bond interactions differ from those of **1**. Atoms O(2)-H…O(3) continue involved in intramolecular hydrogen bonds [O(2)-O(3) 2.5918(13) Å, H(2O)-O(3) 1.76(2) Å and O(2)-H(2O)-O(3) 151.2(19)°], but the intermolecular hydrogen bonds observed are only: [N(3)-O(1) 2.9345(15) Å, H(3N)-O(1) 2.172(18) and N(3)-H(3N)-O(1) 147.8(15)°]. The bond distances found for mhcppe and dbcpe are within the expected range and some selected bond distances and angles are included in Table 1 and more details are given in the ESI section.

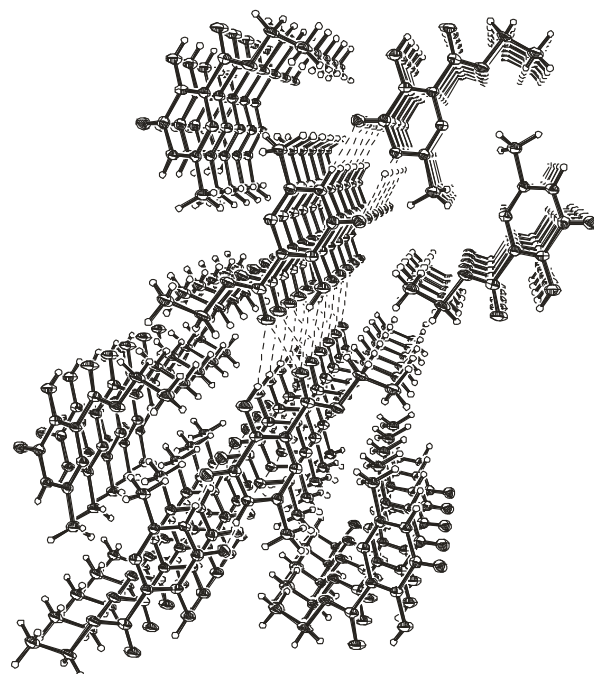


Figure S-10-1 π - π -stacking and hydrogen bonding interactions in the crystal packing of **1** (*mhcppe*).

In the crystal packing of **3**, N-MeHOPY, the distance between centroids of pyrimidinone rings is 3.616 Å. The rings adopt an anti disposition probably due to steric requirements (see Fig. S-10-2). Aromatic-aromatic intermolecular interactions are present in the crystal packing of the crystals of mhcppe and of N-MeHOPY. In the crystal packing of mhcppe we observe an offset-face-

to-face (OFF) interaction with a distance between the centre of both rings of 4.442 Å, but the distance of the pyrimidinone centroid to the N(2) atom of the next ring is 3.598 Å and with the closest atom to atom contact is 3.389 Å.⁵⁸

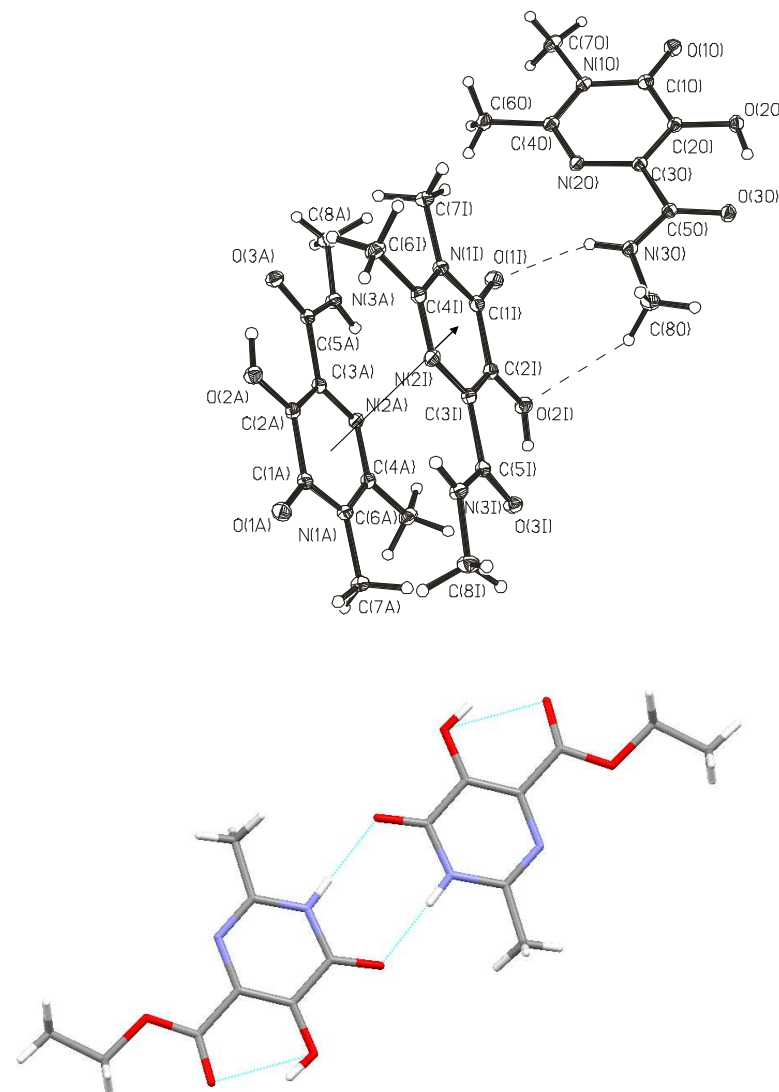
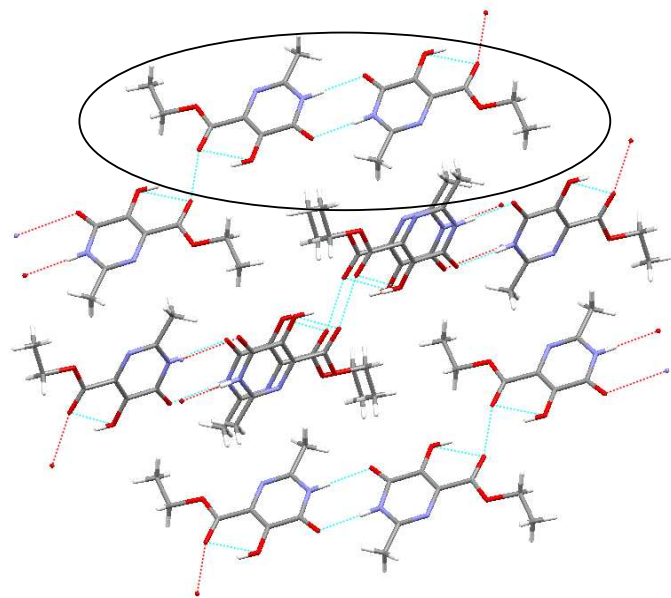
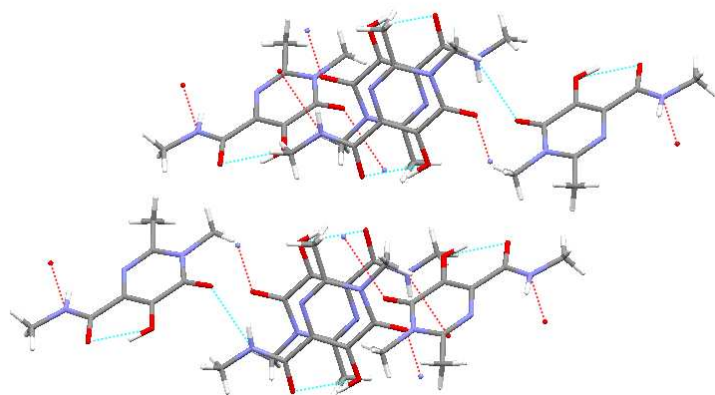


Fig. S-10-2 Two views of the intermolecular H-bonded and π - π -stacking in the solid state of compound 3 (N-MeHOPY).



mhcpe (1)



N-MeHOPY (3)

Fig. S-10-3 A comparative view of the π - π -stacking and hydrogen bonding interactions in the crystal packing of **1** (mhcpe) and of **3** (N-MeHOPY). In the oval circle we can observe the H-bonded ‘dimer’ in the solid-state view in mhcpe.

Table S-10-2 Selected bond angles ($^{\circ}$) for **1** (mhcpe), **2** (dbcpe) and **3** (N-MeHOPY).

1 - mhcpe	2 - dbcpe	3 - N-MeHOPY
Angles ($^{\circ}$)		
C(4)-N(1)-C(1)	124.6(2)	122.49(10)
C(4)-N(2)-C(3)	117.0(3)	118.30(11)
O(1)-C(1)-N(1)	121.1(3)	121.99(11)
O(1)-C(1)-C(2)	125.6(3)	124.07(12)
N(1)-C(1)-C(2)	113.4(3)	113.94(10)
O(2)-C(2)-C(3)	126.3(3)	124.40(11)
O(2)-C(2)-C(1)	114.8(3)	116.15(11)
C(2)-C(3)-N(2)	123.9(3)	123.10(11)
N(2)-C(3)-C(6)	116.6(3)	116.65(10)
N(2)-C(4)-N(1)	122.3(3)	122.70(11)
N(2)-C(4)-C(5)	121.5(3)	118.95(11)
N(1)-C(4)-C(5)	116.2(3)	118.34(11)
O(3)-C(6)-C(3)	122.3(3)	120.49(11)

Table S-10-3A Atomic coordinates ($\times 10^4$) and equivalent isotropic displacement parameters ($\text{\AA}^2 \times 10^3$) for mhcp (1). U(eq) is defined as one third of the trace of the orthogonalized U^{ij} tensor.

	x	y	z	U(eq)
O(1)	3225(1)	13261(5)	5462(1)	42(1)
O(2)	4174(1)	11729(5)	5292(2)	43(1)
O(3)	4590(1)	8156(6)	4414(2)	50(1)
O(4)	4023(1)	5310(5)	3303(2)	42(1)
N(1)	2762(1)	9932(5)	4374(2)	33(1)
N(2)	3161(1)	6876(5)	3633(2)	32(1)
C(1)	3231(1)	11340(7)	4918(2)	33(1)
C(2)	3709(1)	10350(7)	4779(2)	32(1)
C(3)	3652(1)	8185(7)	4154(2)	30(1)
C(4)	2734(1)	7790(7)	3755(2)	30(1)
C(5)	4137(1)	7220(7)	3982(2)	35(1)
C(6)	2180(1)	6607(8)	3207(2)	41(1)
C(7)	4481(1)	4371(8)	3080(2)	46(1)
C(8)	4246(1)	2660(9)	2218(2)	54(1)

Table S-10-3B Atomic coordinates ($\times 10^4$) and equivalent isotropic displacement parameters ($\text{\AA}^2 \times 10^3$) for dbcpe 2. U(eq) is defined as one third of the trace of the orthogonalized U^{ij} tensor.

	x	y	z	U(eq)
O(1)	3626(2)	8384(3)	-38(1)	88(1)
O(2)	2367(2)	6811(3)	1030(1)	70(1)
O(3)	-535(2)	8388(4)	1644(1)	125(1)
O(4)	1315(2)	8621(3)	2303(1)	86(1)
N(1)	2441(2)	10724(3)	57(1)	58(1)
N(2)	881(2)	10876(3)	850(1)	60(1)
C(1)	2803(3)	9108(4)	250(2)	60(1)
C(2)	2137(3)	8411(4)	810(2)	58(1)
C(3)	1239(3)	9332(4)	1086(1)	55(1)
C(4)	1491(3)	11536(4)	354(2)	58(1)
C(5)	3147(3)	11533(5)	-488(2)	89(1)
C(6)	3622(3)	6535(4)	1413(3)	103(1)
C(7)	3718(3)	4750(4)	1625(2)	63(1)
C(8)	4496(3)	3687(5)	1308(2)	79(1)
C(9)	4600(3)	2022(6)	1525(2)	90(1)
C(10)	3915(4)	1463(5)	2043(2)	84(1)
C(11)	3128(4)	2492(6)	2346(2)	86(1)
C(12)	3046(3)	4116(5)	2139(2)	77(1)
C(13)	558(3)	8692(4)	1693(2)	69(1)
C(14)	771(4)	8106(6)	2956(2)	112(2)
C(15)	1707(4)	8309(7)	3559(2)	145(2)
C(16)	1147(3)	13251(4)	107(2)	81(1)

Table S-10-3C Atomic coordinates ($\times 10^4$) and equivalent isotropic displacement parameters ($\text{\AA}^2 \times 10^3$) for N-MeHOPY (**3**). U(eq) is defined as one third of the trace of the orthogonalized U_{ij} tensor.

	x	y	z	U(eq)
N(1)	2004(1)	9907(1)	1037(1)	19(1)
O(1)	2671(1)	8570(1)	2445(1)	25(1)
C(1)	2664(1)	8984(2)	1623(1)	19(1)
O(2)	3971(1)	7666(1)	1699(1)	22(1)
C(2)	3325(1)	8574(2)	1167(1)	18(1)
N(2)	2592(1)	10030(1)	-278(1)	18(1)
O(3)	4549(1)	7831(1)	196(1)	22(1)
C(3)	3262(1)	9114(2)	251(1)	17(1)
N(3)	3807(1)	9294(2)	-1116(1)	20(1)
C(4)	1992(1)	10389(2)	112(1)	19(1)
C(5)	3929(1)	8696(2)	-230(1)	17(1)
C(6)	1251(1)	11343(2)	-462(1)	25(1)
C(7)	1308(1)	10365(2)	1447(1)	25(1)
C(8)	4393(1)	9051(2)	-1693(1)	25(1)

Table S-10-4A Bond lengths [\AA] and angles [$^\circ$] for mhcpe (**1**).

	Bond lengths [\AA]		Angles [$^\circ$]
O(1)-C(1)	1.222(4)	C(2)-O(2)-H(2O)	110(3)
O(2)-C(2)	1.330(3)	C(5)-O(4)-C(7)	116.4(2)
O(2)-H(2O)	0.85(4)	C(4)-N(1)-C(1)	124.6(2)
O(3)-C(5)	1.196(4)	C(4)-N(1)-H(1A)	117.7
O(4)-C(5)	1.317(4)	C(1)-N(1)-H(1A)	117.7
O(4)-C(7)	1.448(3)	C(4)-N(2)-C(3)	117.0(3)
N(1)-C(4)	1.354(4)	O(1)-C(1)-N(1)	121.1(3)
N(1)-C(1)	1.357(4)	O(1)-C(1)-C(2)	125.6(3)
N(1)-H(1A)	0.86	N(1)-C(1)-C(2)	113.4(3)
N(2)-C(4)	1.282(4)	O(2)-C(2)-C(3)	126.3(3)
N(2)-C(3)	1.367(4)	O(2)-C(2)-C(1)	114.8(3)
C(1)-C(2)	1.433(4)	C(3)-C(2)-C(1)	118.9(3)
C(2)-C(3)	1.352(4)	C(2)-C(3)-N(2)	123.9(3)
C(3)-C(5)	1.476(4)	C(2)-C(3)-C(5)	119.4(3)
C(4)-C(6)	1.478(4)	N(2)-C(3)-C(5)	116.6(3)
C(6)-H(6A)	0.96	N(2)-C(4)-N(1)	122.3(3)
C(6)-H(6B)	0.96	N(2)-C(4)-C(6)	121.5(3)
C(6)-H(6C)	0.96	N(1)-C(4)-C(6)	116.2(3)
C(7)-C(8)	1.481(4)	O(3)-C(5)-O(4)	123.7(3)
C(7)-H(7A)	0.97	O(3)-C(5)-C(3)	122.3(3)
C(7)-H(7B)	0.97	O(4)-C(5)-C(3)	113.9(3)
C(8)-H(8A)	0.96	C(4)-C(6)-H(6A)	109.5
C(8)-H(8B)	0.96	C(4)-C(6)-H(6B)	109.5
C(8)-H(8C)	0.96	H(6A)-C(6)-H(6B)	109.5
		C(4)-C(6)-H(6C)	109.5
		H(6A)-C(6)-H(6C)	109.5
		H(6B)-C(6)-H(6C)	109.5
		O(4)-C(7)-C(8)	106.9(2)
		O(4)-C(7)-H(7A)	110.3
		C(8)-C(7)-H(7A)	110.3
		O(4)-C(7)-H(7B)	110.3
		C(8)-C(7)-H(7B)	110.3
		H(7A)-C(7)-H(7B)	108.6
		C(7)-C(8)-H(8A)	109.5
		C(7)-C(8)-H(8B)	109.5
		H(8A)-C(8)-H(8B)	109.5
		C(7)-C(8)-H(8C)	109.5
		H(8A)-C(8)-H(8C)	109.5
		H(8B)-C(8)-H(8C)	109.5

Table S-10-4B Bond lengths [\AA] and angles [$^\circ$] for dbcpe (**2**).

Bond lengths [\AA]		Angles [$^\circ$]	
O(1)-C(1)	1.226(3)	C(2)-O(2)-C(6)	114.3(2)
O(2)-C(2)	1.366(3)	C(13)-O(4)-C(14)	117.7(3)
O(2)-C(6)	1.454(4)	C(4)-N(1)-C(1)	122.4(3)
O(3)-C(13)	1.182(3)	C(4)-N(1)-C(5)	121.5(3)
O(4)-C(13)	1.310(4)	C(1)-N(1)-C(5)	116.1(3)
O(4)-C(14)	1.465(4)	C(4)-N(2)-C(3)	117.3(2)
N(1)-C(4)	1.374(3)	O(1)-C(1)-N(1)	121.5(3)
N(1)-C(1)	1.393(4)	O(1)-C(1)-C(2)	124.5(3)
N(1)-C(5)	1.482(4)	N(1)-C(1)-C(2)	113.9(3)
N(2)-C(4)	1.302(3)	C(3)-C(2)-O(2)	120.8(3)
N(2)-C(3)	1.359(4)	C(3)-C(2)-C(1)	119.3(3)
C(1)-C(2)	1.442(4)	O(2)-C(2)-C(1)	119.8(3)
C(2)-C(3)	1.357(4)	C(2)-C(3)-N(2)	124.1(3)
C(3)-C(13)	1.502(4)	C(2)-C(3)-C(13)	121.3(3)
C(4)-C(16)	1.488(4)	N(2)-C(3)-C(13)	114.6(3)
C(6)-H(5A)	0.96	N(2)-C(4)-N(1)	122.9(3)
C(6)-H(5B)	0.96	N(2)-C(4)-C(16)	118.2(3)
C(6)-H(5C)	0.96	N(1)-C(4)-C(16)	118.9(3)
C(6)-C(7)	1.492(4)	N(1)-C(5)-H(5A)	109.5
C(6)-H(6A)	0.97	N(1)-C(5)-H(5B)	109.5
C(6)-H(6B)	0.97	H(5A)-C(5)-H(5B)	109.5
C(7)-C(8)	1.372(4)	N(1)-C(5)-H(5C)	109.5
C(8)-C(9)	1.401(5)	H(5A)-C(5)-H(5C)	109.5
C(8)-H(8A)	0.93	H(5B)-C(5)-H(5C)	109.5
C(7)-C(12)	1.358(4)	O(2)-C(6)-C(7)	107.8(2)
C(9)-C(10)	1.353(5)	O(2)-C(6)-H(6A)	110.1
C(9)-H(9A)	0.93	C(7)-C(6)-H(6A)	110.1
C(10)-C(11)	1.347(5)	O(2)-C(6)-H(6B)	110.1
C(10)-H(10A)	0.93	C(7)-C(6)-H(6B)	110.1
C(11)-C(12)	1.364(5)	H(6A)-C(6)-H(6B)	108.5
C(11)-H(11A)	0.93	C(12)-C(7)-C(8)	117.5(3)
C(11)-H(12A)	0.93	C(12)-C(7)-C(6)	121.5(3)
C(14)-C(15)	1.417(5)	C(8)-C(7)-C(6)	121.0(3)
C(14)-H(14A)	0.97	C(7)-C(8)-C(9)	120.4(3)
C(14)-H(14B)	0.97	C(7)-C(8)-H(8A)	119.8
C(15)-H(15A)	0.96	C(9)-C(8)-H(8A)	119.8
C(15)-H(15B)	0.96	C(10)-C(9)-C(8)	119.5(3)
C(15)-H(15C)	0.96	C(10)-C(9)-H(9A)	120.2
C(16)-H(16A)	0.96	C(8)-C(9)-H(9A)	120.2
C(16)-H(16B)	0.96	C(11)-C(10)-C(9)	120.4(4)
C(16)-H(16C)	0.96	C(11)-C(10)-H(10A)	119.8
		C(9)-C(10)-H(10A)	119.8
		C(10)-C(11)-C(12)	119.6(4)
		C(10)-C(11)-H(11A)	120.2
		C(12)-C(11)-H(11A)	120.2
		C(7)-C(12)-C(11)	122.5(3)
		C(7)-C(12)-H(12A)	118.7
		C(11)-C(12)-H(12A)	118.7

O(3)-C(13)-O(4)	123.7(3)
O(3)-C(13)-C(3)	124.8(3)
O(4)-C(13)-C(3)	111.3(3)
C(15)-C(14)-O(4)	108.2(3)
C(15)-C(14)-H(14A)	110.1
O(4)-C(14)-H(14A)	110.1
C(15)-C(14)-H(14B)	110.1
O(4)-C(14)-H(14B)	110.1
H(14A)-C(14)-H(14B)	108.4
C(14)-C(15)-H(15A)	109.5
C(14)-C(15)-H(15B)	109.5
H(15A)-C(15)-H(15B)	109.5
C(14)-C(15)-H(15C)	109.5
H(15A)-C(15)-H(15C)	109.5
H(15B)-C(15)-H(15C)	109.5
C(4)-C(16)-H(16A)	109.5
C(4)-C(16)-H(16B)	109.5
H(16A)-C(16)-H(16B)	109.5
C(4)-C(16)-H(16C)	109.5
H(16A)-C(16)-H(16C)	109.5
H(16B)-C(16)-H(16C)	109.5

Table S-10-4C Bond lengths [\AA] and angles [$^\circ$] for N-MeHOPY (**3**).

Bond lengths [\AA]	Angles [$^\circ$]
N(1)-C(4)	1.3798(16)
N(1)-C(1)	1.3965(16)
N(1)-C(7)	1.4729(16)
O(1)-C(1)	1.2259(15)
C(1)-C(2)	1.4549(17)
O(2)-C(2)	1.3463(15)
C(2)-C(3)	1.3634(17)
N(2)-C(4)	1.2962(16)
N(2)-C(3)	1.3740(15)
O(3)-C(5)	1.2504(15)
C(3)-C(5)	1.4878(16)
N(3)-C(5)	1.3256(16)
N(3)-C(8)	1.4478(16)
C(4)-C(6)	1.4913(18)
	C(4)-N(1)-C(1)
	C(4)-N(1)-C(7)
	C(1)-N(1)-C(7)
	O(1)-C(1)-N(1)
	O(1)-C(1)-C(2)
	C(1)-C(1)-C(2)
	N(1)-C(1)-C(2)
	O(2)-C(2)-C(3)
	O(2)-C(2)-C(1)
	C(2)-C(2)-C(1)
	C(3)-C(2)-C(1)
	C(4)-N(2)-C(3)
	C(2)-C(3)-N(2)
	C(2)-C(3)-C(5)
	N(2)-C(3)-C(5)
	C(5)-N(3)-C(8)
	C(5)-N(3)-C(4)
	N(2)-C(4)-N(1)
	N(2)-C(4)-C(6)
	N(1)-C(4)-C(6)
	O(3)-C(5)-N(3)
	O(3)-C(5)-C(3)
	N(3)-C(5)-C(3)

Table S-10-5A Anisotropic displacement parameters ($\text{\AA}^2 \times 10^3$) for mhcpe (**1**). The anisotropic displacement factor exponent takes the form: $-2p^2[h^2 a^*{}^2U^{11} + \dots + 2 h k a^* b^* U^{12}]$

	U ¹¹	U ²²	U ³³	U ²³	U ¹³	U ¹²
O(1)	35(1)	47(1)	46(1)	-12(1)	19(1)	-2(1)
O(2)	23(1)	51(2)	51(2)	-14(1)	11(1)	-4(1)
O(3)	20(1)	61(2)	66(2)	-16(1)	13(1)	-3(1)
O(4)	23(1)	53(2)	55(1)	-15(1)	20(1)	-1(1)
N(1)	21(1)	40(2)	37(2)	-2(1)	13(1)	4(1)
N(2)	23(1)	38(2)	35(2)	0(1)	11(1)	1(1)
C(1)	30(2)	33(2)	35(2)	3(1)	13(1)	0(1)
C(2)	22(1)	36(2)	35(2)	0(1)	9(1)	-1(1)
C(3)	21(1)	35(2)	34(2)	3(1)	10(1)	1(1)
C(4)	26(2)	34(2)	31(2)	5(1)	12(1)	2(1)
C(5)	25(2)	38(2)	45(2)	1(2)	15(1)	1(1)
C(6)	24(2)	52(2)	45(2)	-6(2)	12(1)	1(1)
C(7)	23(2)	60(2)	61(2)	-9(2)	24(2)	3(2)
C(8)	29(2)	76(3)	59(2)	-15(2)	20(2)	3(2)

Table S-10-5B Anisotropic displacement parameters ($\text{\AA}^2 \times 10^3$) for dbcpe (**2**), The anisotropic displacement factor exponent takes the form: $-2p^2[h^2 a^*{}^2U^{11} + \dots + 2 h k a^* b^* U^{12}]$

	U ¹¹	U ²²	U ³³	U ²³	U ¹³	U ¹²
O(1)	72(2)	105(2)	91(2)	-8(1)	23(1)	25(1)
O(2)	57(1)	53(1)	97(2)	5(1)	-10(1)	1(1)
O(3)	69(2)	216(3)	90(2)	22(2)	9(1)	-43(2)
O(4)	77(1)	120(2)	61(1)	21(1)	4(1)	-30(1)
N(1)	50(1)	70(2)	54(1)	5(1)	5(1)	5(1)
N(2)	59(1)	60(2)	60(2)	1(1)	8(1)	8(1)
C(1)	52(2)	71(2)	56(2)	-5(2)	3(2)	6(2)
C(2)	50(2)	55(2)	64(2)	-3(2)	-5(1)	-1(1)
C(3)	52(2)	62(2)	51(2)	-2(2)	4(1)	-4(2)
C(4)	56(2)	60(2)	55(2)	-2(2)	-3(2)	3(2)
C(5)	68(2)	123(3)	77(2)	27(2)	22(2)	6(2)
C(6)	64(2)	74(3)	161(4)	33(2)	-31(2)	-4(2)
C(7)	45(2)	57(2)	83(2)	5(2)	-4(2)	2(2)
C(8)	61(2)	103(3)	74(2)	1(2)	12(2)	-2(2)
C(9)	67(2)	87(3)	114(3)	-33(3)	1(2)	23(2)
C(10)	80(2)	62(2)	102(3)	3(2)	-25(2)	4(2)
C(11)	93(3)	80(3)	84(2)	2(2)	10(2)	-15(2)
C(12)	68(2)	69(3)	97(3)	-18(2)	22(2)	2(2)
C(13)	62(2)	75(2)	68(2)	-1(2)	4(2)	-10(2)
C(14)	99(3)	165(4)	72(2)	40(3)	17(2)	-28(3)
C(15)	106(3)	260(7)	67(3)	19(3)	8(2)	-29(4)
C(16)	92(2)	68(2)	83(2)	14(2)	10(2)	13(2)

Table S-10-5C Anisotropic displacement parameters ($\text{\AA}^2 \times 10^3$) for N-MeHOPY (**3**).
 The anisotropic displacement factor exponent takes the form: $-2p^2[h^2 a^*2U^{11} + \dots + 2hka^*b^*U^{12}]$

	U ¹¹	U ²²	U ³³	U ²³	U ¹³	U ¹²
N(1)	16(1)	21(1)	21(1)	-4(1)	7(1)	-2(1)
O(1)	26(1)	32(1)	19(1)	-1(1)	8(1)	-2(1)
C(1)	19(1)	19(1)	19(1)	-4(1)	5(1)	-3(1)
O(2)	20(1)	26(1)	20(1)	3(1)	4(1)	3(1)
C(2)	16(1)	17(1)	19(1)	-2(1)	3(1)	-1(1)
N(2)	16(1)	18(1)	21(1)	0(1)	5(1)	0(1)
O(3)	19(1)	24(1)	22(1)	1(1)	6(1)	5(1)
C(3)	16(1)	16(1)	19(1)	-3(1)	5(1)	-2(1)
N(3)	17(1)	24(1)	19(1)	2(1)	6(1)	2(1)
C(4)	18(1)	16(1)	23(1)	-3(1)	5(1)	-2(1)
C(5)	17(1)	16(1)	19(1)	-2(1)	5(1)	-2(1)
C(6)	19(1)	24(1)	32(1)	2(1)	5(1)	4(1)
C(7)	20(1)	29(1)	30(1)	-7(1)	12(1)	0(1)
C(8)	26(1)	31(1)	22(1)	1(1)	12(1)	2(1)

Table S-10-6A Hydrogen coordinates ($\times 10^4$) and isotropic displacement parameters ($\text{\AA}^2 \times 10^3$) for mhcp (1).

	x	y	z	U(eq)
H(2O)	4439(16)	10980(90)	5190(20)	68(13)
H(1A)	2461	10436	4425	39
H(6A)	2213	4748	2926	61
H(6B)	1983	8042	2745	61
H(6C)	1984	6261	3593	61
H(7A)	4731	3111	3560	55
H(7B)	4682	6112	3009	55
H(8A)	4538	1937	2058	81
H(8B)	4009	3951	1745	81
H(8C)	4038	984	2293	81

Table S-10-6B Hydrogen coordinates ($\times 10^4$) and isotropic displacement parameters ($\text{\AA}^2 \times 10^3$) for dbcpe (**2**).

	x	y	z	U(eq)
H(5A)	2820	12630	-587	133
H(5B)	3052	10893	-927	133
H(5C)	4028	11599	-304	133
H(6A)	3751	7233	1841	123
H(6B)	4263	6807	1102	123
H(8A)	4957	4073	948	95
H(9A)	5136	1307	1314	108
H(10A)	3988	362	2192	101
H(11A)	2643	2096	2693	103
H(12A)	2511	4817	2358	93
H(14A)	35	8778	3017	134
H(14B)	508	6954	2914	134
H(15A)	1372	7959	3992	217
H(15B)	1947	9456	3603	217
H(15C)	2434	7649	3491	217
H(16A)	475	13655	361	121
H(16B)	874	13243	-404	121
H(16C)	1872	13962	205	121

Table S-10-6C Hydrogen coordinates ($\times 10^4$) and isotropic displacement parameters ($\text{\AA}^2 \times 10^3$) for N-MeHOPY (**3**).

	x	y	z	U(eq)
H(2O)	4315(13)	7540(30)	1309(16)	52(6)
H(3N)	3361(11)	9860(20)	-1370(12)	33(4)
H(6C)	741(10)	10630(20)	-555(11)	30(4)
H(6B)	1357(11)	11600(20)	-1062(13)	38(5)
H(6A)	1133(11)	12360(20)	-142(13)	37(5)
H(7C)	824(12)	9810(30)	1084(14)	44(5)
H(7B)	1247(12)	11580(30)	1442(13)	48(5)
H(7A)	1426(12)	9980(30)	2105(15)	56(6)
H(8C)	4893(13)	8620(30)	-1308(14)	51(6)
H(8B)	4166(13)	8240(30)	-2219(14)	52(6)
H(8A)	4508(12)	10110(30)	-1961(13)	45(5)